united nations
educational, scientific
and cultural
organization

international atomic
energy agency

the
abdus salam
international centre for theoretical physics

SMR: 1133/8

WINTER COLLEGE ON
SPECTROSCOPY AND APPLICATIONS

(8 - 26 February 1999)

"Biomedical Applications of Spectroscopy"

presented by:

Sune SVANBERG
Lund Institute of Technology
Division of Atomic Physics
Lund
Sweden

96-50

Physica Scripta. Vol. T72, 69–75, 1997.

New Developments in Laser Medicine

S. Svanberg

Lund Laser Centre, Lund University, P.O. Box 118, S-221 00 Lund, Sweden and Department of Physics, Lund Institute of Technology, P.O. Box 118, S-221 00 Lund, Sweden

Received July 17, 1996; accepted November 8, 1996

Abstract

New developments in the non-thermal application of laser radiation in medicine are discussed. Tumour-seeking agents in combination with laser light are used for early tumour detection through fluorescence and for photodynamic therapy. Laser-induced fluorescence as well as Raman spectroscopy has potential for real-time monitoring of atherosclerotic plaques. Enhanced demarcation can be obtained by working in the time domain, which also opens up the new field of photon propagation studies in tissue. Work towards optical mammography is in progress in many laboratories. Finally, intense laser pulses can be used for generating X-ray radiation with interesting properties for enhanced medical imaging.

1.-Introduction

Laser technology provides many applications in medicine, both with regard to diagnostics and to therapy [1–3]. Originally, thermal interactions strongly dominated the scene providing new possibilities in surgery and haemostasis. Thermal applications are still the most important and have become more and more sophisticated, partly because of improved modelling of light interaction with tissue (See, e.g. [4]). However, during recent years several new, more spectroscopically oriented modalities have emerged, and an overview of this field, using examples from work at the Lund University Medical Laser Centre [5], will be given.

Photodynamic therapy is a photochemical treatment modality, where tumour-seeking agents are used in conjunction with red laser light with non-hyperthermic intensities [6–8]. While this type of therapy has been pursued for quite some time, this modality has become much more realistic during recent years, partly because of the introduction of new sensitizers, such as δ-amino levulinic acid (ALA).

Laser spectroscopic techniques are providing new possibilities for tissue diagnostics [9, 10]. Laser-induced fluorescence spectra for biological molecules have comparatively little structure, but sometimes have sufficient specificity to allow demarcation between diseased and surrounding normal tissue. This is particularly true if tumour marking has been performed with tumour-seeking agents. Atherosclerotically transformed vessel wall can also be identified providing means for spectroscopic guidance of angioplasty. Apart from time-integrated monitoring of the full fluorescence spectra, time-resolved data can be obtained to enhance demarcation capability. Raman spectra are much weaker but have a higher specificity, giving future hope for very selective optical biopsy sampling. Fluorescence instrumentation for point monitoring and imaging have been developed and examples from different clinical specialities are given.

Elastically scattered light can also be used for tissue analysis. Thus, tissue blood perfusion can be assessed by laser Doppler flowmetry [11], which now is also able to generate blood-flow images. Photon migration studies in tissue constitute a strongly developing field [12]. By time-resolved spectroscopy it is possible to follow the transport of photons through tissue. In particular, time-resolved transillumination with detection of only the first emerging photons allows enhanced viewing through tissue by reducing the image blurring due to multiple light scattering. Much research work is focussed on the development of mammography without employing ionizing radiation. Other aspects of photon migration in tissue are optical dosimetry for successful photodynamic treatment of malignant tumours, and studies of brain oxygenation.

Using focussed high-power laser pulses impinging on high nuclear-charge targets, ultra-short intense bursts of hard X-ray radiation are generated. Such sources of X-rays may provide new possibilities in medical diagnostics, where the ultra-fine source size and short pulse duration may be utilized for sharper imaging with potentially lower does [13].

We will in the following sections discuss certain new aspects of lasers in medicine as indicated above. Finally, the future prospects of the techniques are discussed.

2.-Tumour photodynamic therapy and diagnostics

Tissue molecules, irradiated by laser light, can release their excess energy either through radiationless transitions (heat), through photochemical processes, or emission of fluorescence radiation. Optical treatment of psoriasis patients, or new-born infants with an excess of bilirubin, are well-known examples of medical photochemistry. Photodynamic tumour therapy (PDT) using tumour-seeking agents is a further example of special interest in our context. By optical excitation of a sensitizing molecule, energy can be transferred to oxygen molecules in the tissue, which are excited into their aggressive singlet state. Selective singlet oxygen release gives rise to the death of malignant cells, where the drug accumulated. A large number of sensitizing agents, such as haematoporphyrin derivatives, phtalocyanines, chlorines and purpurins have been developed and are now in different states of clinical evaluation. Of special interest is the natural biological transformation of δ-amino levulinic acid (ALA) to protoporphyrin IX, which is photo-dynamically very active and also strongly fluorescing [14,15]. ALA is a natural molecule in the body and the normal haem cycle for haem production is utilized (See Fig. 1).

ALA can be given topically, i.e. it can be provided in a cream that is applied superficially over skin tumours, such as basal cell carcinoma. The protoporphyrin build-up can be

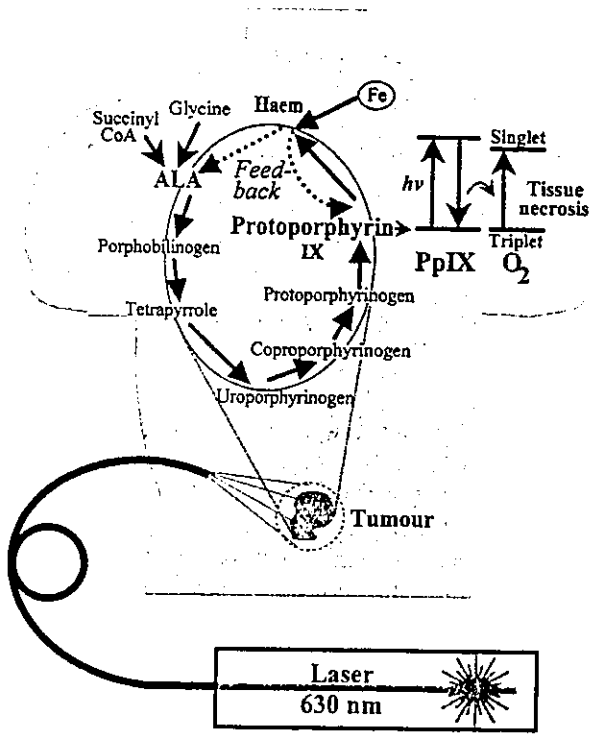

Fig. 1. Schematic diagram of the haem cycle, illustrating the production of protoporphyrin IX from ALA. The transfer of the energy from excited ALA molecules to oxygen molecules is also indicated. (From Ref [15]).

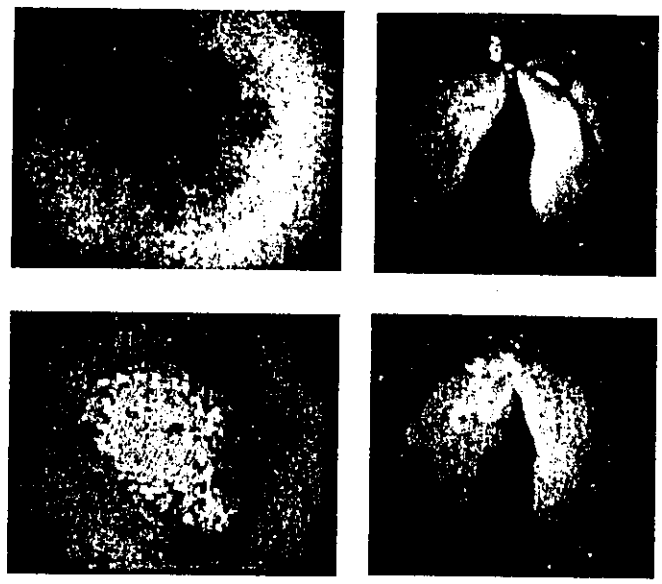

Fig. 3. Fluorescence image of a human basal cell carcinoma (left) and vocal chords (right), represented in false-colour coding, superimposed on the normal colour images. Note the benign naevus to the right of the basal cell carcinoma. No cancer indication is obtained for that lesion. (From Ref [17]).

detected as in Fig. 2, where a strong, dual-peaked signal in the red spectral region is observed in the malignant tissue when excited by UV light from a nitrogen laser. In normal tissue, blue-green fluorescence due to native molecules such as NADH, elastin and collagen is instead dominant. An attractive scheme for tumour detection is to monitor the increase in the red intensity and divide that signal with the blue-green decreasing intensity. In that way an enhanced tumour demarcation is achieved at the same time as the recording of a dimensionless quantity, such as a ratio, gives immunity to influences due to variations in tissue topography, intensity fluctuations etc. We have developed a clinical multi-colour imaging system [16,17], where a false-coloured ratio image is superimposed on the normal colour image of the tissue under investigation. Examples of clinical tumour imaging are shown in Fig. 3.

Photodynamic therapy is achieved by irradiating the tissue by red light; at 635 nm for the case of ALA-PDT. A photograph illustrating clinical treatment of basal cell carcinoma at the Medical Laser Centre, Lund University, is shown in Fig. 4. Photographs showing superficial and nodular basal-cell carcinoma before and after treatment are presented in Fig. 5. PDT can also be applied to a variety of other locations, such as the lung, bladder and ENT region.

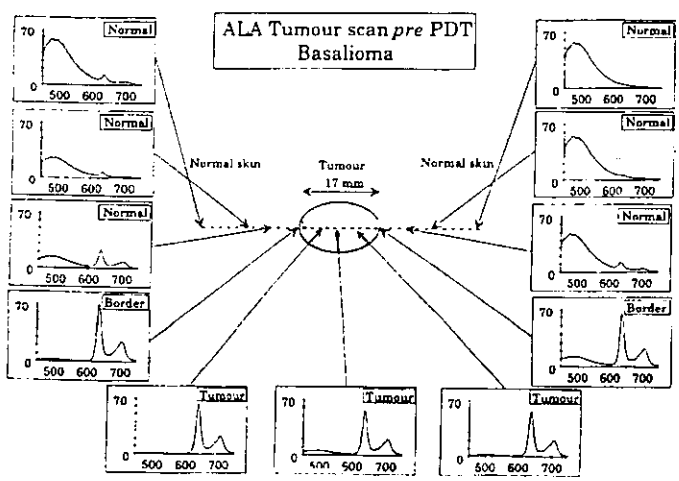

Fig. 2. Fluorescence spectra recorded at different positions along a line through a human basal-cell carcinoma. The skin area had been subjected to an ALA-containing cream 6 hours before the investigation. (From Ref [15]).

3.-Vascular monitoring and treatment

Cardiovascular disease is, besides cancer, the major cause of death in Western countries. The surgical treatment of severe atherosclerosis includes aggressive procedures, such as open-

Fig. 4. Photograph of clinical PDT at the Lund University Medical Laser Centre. (From Ref [18]).

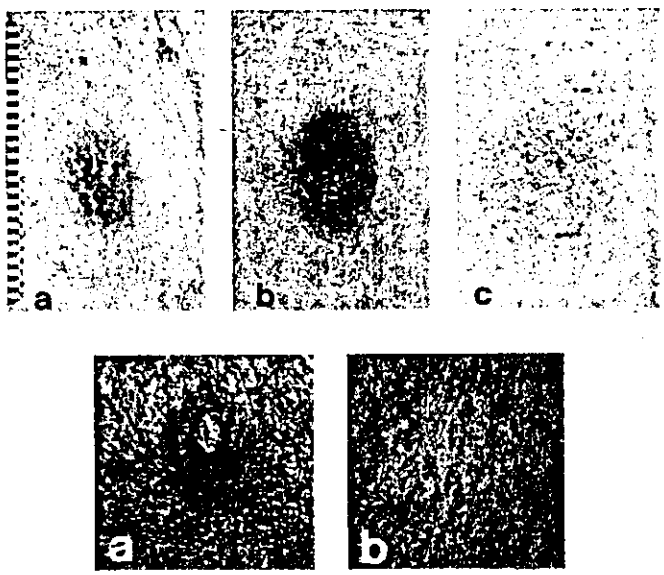

Fig. 5. ALA-PDT treatment of human basal cell carcinoma. Upper row: superficial basal cell carcinoma before (a), 1 week after (b) and three weeks after PDT. Lower row: nodular basal cell carcinoma before (a) and 4 months after PDT (b). (From Ref [15]).

heart surgery with coronary by-pass operation. Several new modalities are now being investigated as possible replacements for such extensive procedures. A new modality is laser based transluminal angioplasty, in which fiber based catheters through a peripheral artery, e.g. the femoral artery, are used as an entrance for intra vasal treatment. A schematic diagram of such a procedure is shown in Fig. 6 [18]. It is possible to distinguish atherosclerotic lesions from non-diseased vessel wall using laser-induced fluorescence. The spectral shape of the tissue fluorescence reflects a change in molecular contents. In the insert in the figure it is shown how the spectrum is influenced when elastin is partly replaced by collagen in plaque. In both spectra, a minimum in the fluorescence signal can be seen at 420 nm, representing the strong absorption of haemoglobin in blood. Weaker absorption peaks occur at 540 and 580 nm. Clearly, the influence of the blood reabsorption must be handled properly by a reliable fluorescence diagnostic system. This can be done by forming a ratio of intensities for a wavelength pair corresponding to equal blood absorptions. Fluorescence provides a completely non- intrusive way of probing prior to firing a high-power pulse if plaque is indicated. At the present time the rate of re-stenosis of the vessels is the same for laser angioplasty as for an established modality of transluminal vessel treatment, balloon dilatation (PTCA). Thus catheters and techniques for laser angioplasty need to be improved.

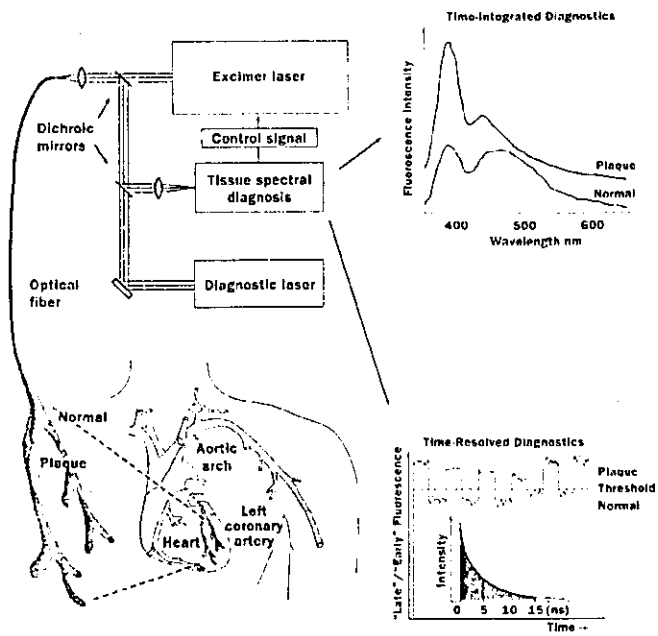

Fig. 6. Schematic diagram of fluorescence diagnostics and interactive laser angioplasty. Experimental spectra for plaque and normal artery wall, as well as recordings of the temporal decay of the fluorescence, represented as the ratio between "late" and "early" fluorescence are given. (Adapted from Ref [18]).

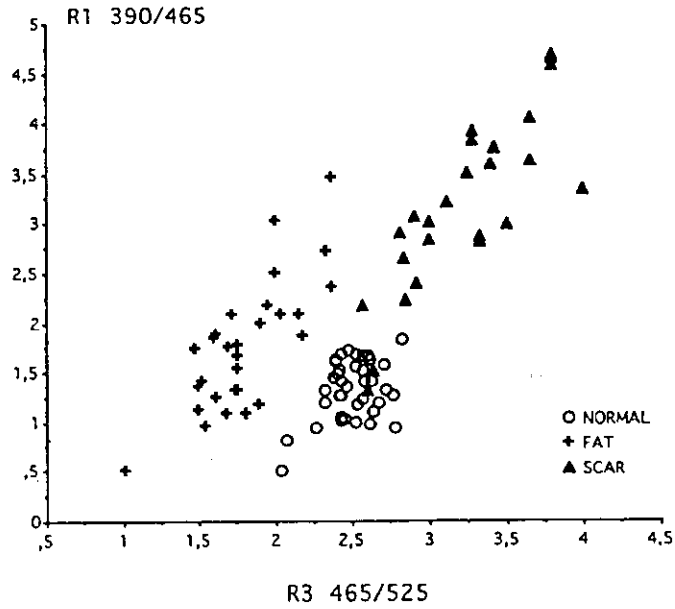

Fig. 7. Two-dimensional diagram showing spectral characteristics of different types of cardiac tissue (in vitro), plotted against two intensity ratios. (From Ref [19]).

Similar techniques can be used for studying myocardial tissue for assessing the status of the heart muscle. From a large number of biopsy samples it was found that normal myocardial tissue can be distinguished from scar or fatty tissue as shown in Fig. 7, where two fluorescence intensity ratios have been used for the demarcation [19].

Raman spectroscopy has long been a powerful tool used by chemists in the analysis of complex organic molecules. The techniques of Raman spectroscopy are now being adopted for tissue spectroscopy. The main difficulty with this technique is the weakness of the signals and the competing process of fluorescence, which normally tends to completely overwhelm the Raman signals which otherwise are attractive because of their sharpness. An efficient way to reduce the influence of fluorescence is to use a laser with a near-IR wavelength, which does not excite fluorescence very efficiently. A CW Nd:YAG laser (λ = 1064 nm) in combination with a Fourier transform spectrometer provides an efficient way of recording Raman spectra. A clinically more practical way is to use a near-IR diode laser in combination with a cooled near-IR CCD array. Raman spectroscopy for plaque diagnostics seems promising [20,21].

4.-Time-resolved tissue fluorescence monitoring

In all the tissue diagnostic measurements discussed so far the total light intensity following pulsed laser excitation has been used. However, the temporal decay characteristics of laser-induced fluorescence may also be utilised for tissue characterisation, e.g. for distinguishing atherosclerotically diseased vessel wall from normal vessel wall. As shown in Fig. 8 the fluorescence from the diseased region has a longer decay time compared to the normal vessel wall tissue [22]. The reason for this is basically that collagen, being more abundant in plaque, has a longer lifetime than elastin. These recordings were taken with an advanced set-up incorporating a mode-locked picosecond laser source in conjunction with time correlating photon-counting electronics. By a detailed analysis it is possible to unfold the decay into three components with different decay times. However, since the lifetimes involved are of the order of ns it is also possible for a clinically practical device to use a normal nitrogen laser with a pulse duration of about 3 ns and use gated integrators to capture "late" fluorescence (5–15 ns) and divide it by "early" fluorescence (0–5 ns). A recording obtained in this way when moving the fibre tip alternatingly between plaque and normal wall is included in Fig. 6.

Decay curves detected at 630 nm for an experimental tumour and surrounding normal issue are also included in Fig. 8. The animal had previously been injected with HPD (Photofrin). It can be seen that the tumour curve has mostly a slow decay component, while normal tissue also exhibits a fast decay. The fast component corresponds to the tissue autofluorescence, whereas the more long-lived component is due to the HPD drug. Enhanced tumour detection can be obtained in fluorescence imaging where fast temporal gating of an image intensifier is used, restricting the detection to late times on each transient.

Fluorescence can be suppressed when Raman spectroscopy is being performed, by using a picosecond laser source and limiting the detection to the duration of these short pulses. Then fluorescence, which typically has a lifetime of a few ns, is reduced while all the Raman photons are recorded, since the latter process is basically instantaneous.

5.-Tissue transillumination — Optical mammography

It is well known that red light penetrates tissue, a fact that is utilized in photo-dynamic therapy. It would then be attractive to use the light transmitted through tissue to perform imaging of e.g. deep-lying tumours without using ionizing radiation. However, light scattering in tissue complicates normal light propagation, since straight beam lines cannot be obtained. Thus, in transillumination no sharp images can normally be obtained because of the strong scattering. Using time-resolved spectroscopy it is possible to follow the photon paths through the tissue after injection of an ultra-short pulse as shown in Fig. 9 [23]. Because of the multiple scattering, most of the photons penetrating the tissue have spent a long time in the tissue, while only very few photons arrive to the detector at the nominal propagation time without disruptions. However, by selecting a very small detection time window and recording the very first photons, it is possible to look at just the "fastest" photons coming out of the tissue. If an obstacle, such as a bone or a tumour blocks the passage, a shadow will be created for the selected subgroup of very early photons.

By scanning the tissue under investigation, a transillumination image can be created. Images of a ductal breast carcinoma in a newly resected breast are given in Fig. 10. A diode laser, operating at 815 nm and producing 30 ps long pulses at a repetition rate of 10 MHz was used. An individual time-dispersion curve, corresponding to a particular location is included. The transmitting and receiving fibers are scanned together under computer control over the tissue, that is compressed between glass plates. In the time-integrated light the tumour cannot be seen. It was also difficult to detect using conventional X-ray mammography. In the time-gated image the tumour can be clearly seen. In order to eliminate possible artefacts it is advantageous to divide the early light by the total light as also shown in the figure [24].

The physics of enhanced imaging through gated viewing is illuminated in Fig. 11, where experimental time histograms from time-resolved transillumination of a 30 mm thick Intralipid phantom are shown [25]. In the top panel the

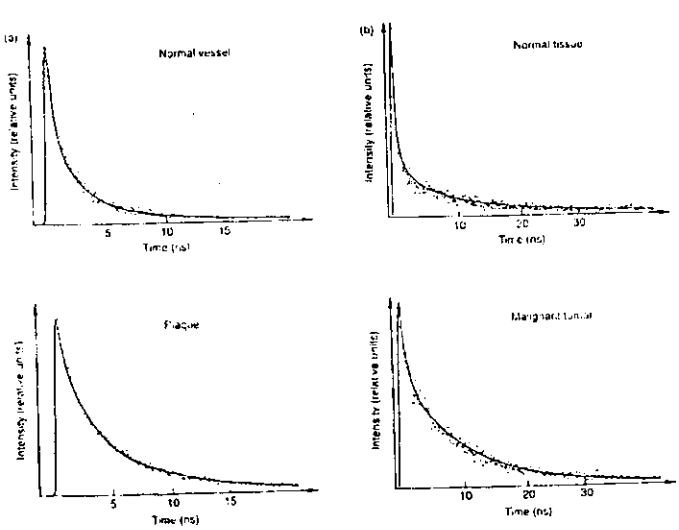

Fig. 8. Temporal decay curves of a) atherosclerotic plaque and normal surrounding tissue, and b) malignant tumour and surrounding normal tissue. (From Ref [22]).

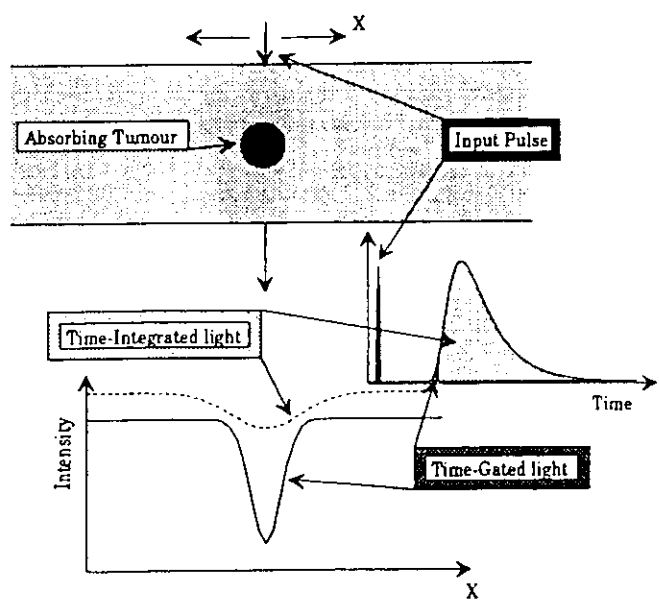

Fig. 9. Principles of time-resolved optical transillumination of tissue. (From Ref [23]).

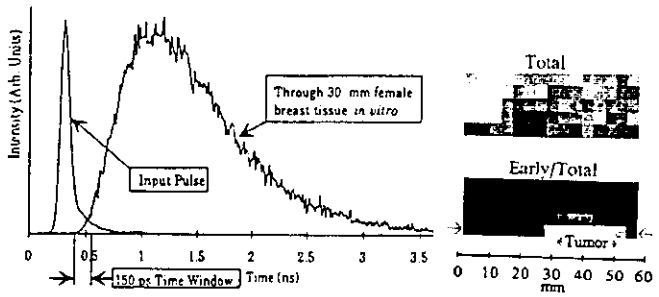

Fig. 10. Transillumination images of breast tissue in vitro showing the presence of a tumour in the prompt light component of the time dispersion curve. A pulsed diode laser was used as a transmitter. (From Ref [24]).

scattering has been increased while keeping the absorption constant, while corresponding curves for fixed scattering but varying absorption are given in the lower panel. We note that the number of early arriving photons is mainly determined by the scattering and not by the absorption. Thus, scattering differences between different types of tissues are important for sharp image formation. Further, the temporal behaviour at late times is mainly governed by the absorptive properties. Thus, time-resolved monitoring is also useful for assessing the concentration of tumour sensitizers in tissue and for monitoring tissue oxygenisation, since the detailed features of the blood absorption depend on the amount of oxy-hemoglobine.

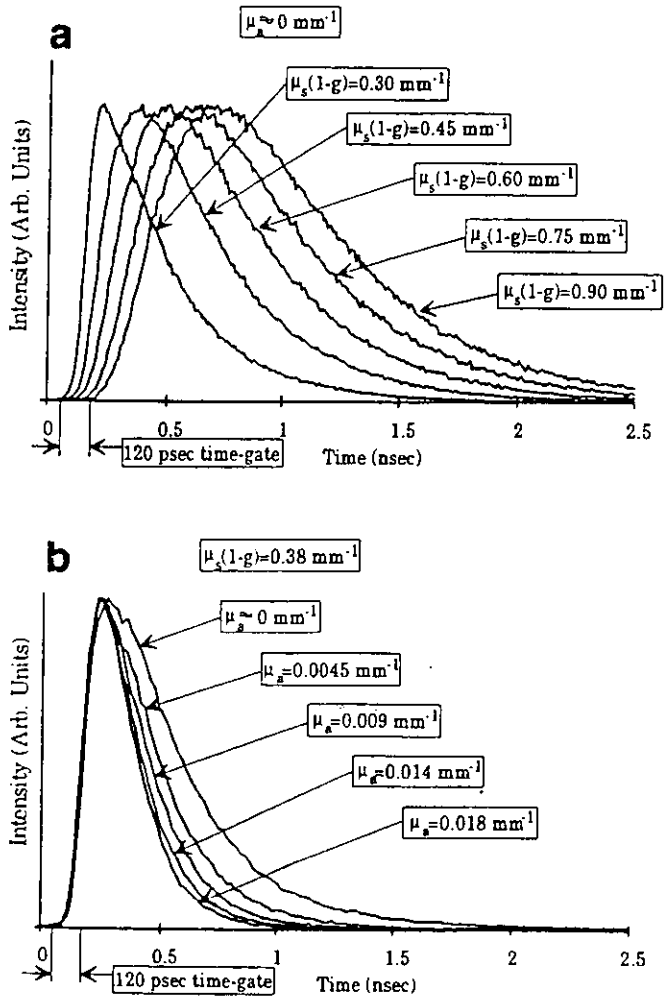

Fig. 11. Time dispersion curves for photons transmitted through a phantom consisting of a 30 mm thick solution of Intralipid and ink. (From Ref [25]).

Many groups are now working in the field of imaging in turbid media, developing a variety of techniques for suppressing excessive scattering, including the use of streak-camera, Raman-amplifier and frequency-doubling gating. Fast modulation of the source followed by detection of phase-shifts and loss of modulation depth can give similar information. The coherence properties of non-scattered light are used in heterodyne and light-in-flight holography. Imaging in scattering media can also be performed with spatial domain reflectometry [12].

6. Imaging with laser-produced X-rays

As we have seen in the previous section there is presently much research aimed at replacing ionizing radiation by optical laser light in certain types of medical imaging. However, intense laser beams can also be utilized for a new generation scheme for X-rays, which can have potential advantages in medicine. The generation of hard X-rays by focussing pulses from a terawatt laser on a high-Z metallic target is illustrated in Fig. 12 [26]. The resulting X-ray source has a minute extension allowing strong magnification radiography to be performed. Normal imaging plates used for digital medical radiography can be employed. A recording of a human Incus (ear bone) and a mesh is shown in Fig. 13, which was obtained using a single laser pulse for X-ray production [27]. Thus, the exposure time is about 10^{-12} s. Also using X-rays through thick media, e.g. the whole body, scattered radiation dominates the radiation arriving at the image plate. X-ray gated viewing should thus be advantageous in X-ray imaging by reducing the noise from the unwanted background. Lower X-ray doses for the same image quality thus seem possible, but only if time-gated X-ray detectors of high efficiency can be developed. Laser-based medical X-rays would also, through change of target material, allow differential imaging of contrast-agent containing objects by making recordings just below and just above the K-absorption edge of the contrast agent in a similar way as presently performed using synchrotron radiation. A first attempt is shown in Fig. 14 for the case of rat stomachs, filled with gadolinium and cerium solutions [13]. The upper image was recorded using a tantalum irradiation target. The lower image was obtained by dividing the first image with a similar image, recorded with a gadolinium target. Because of differential absorption

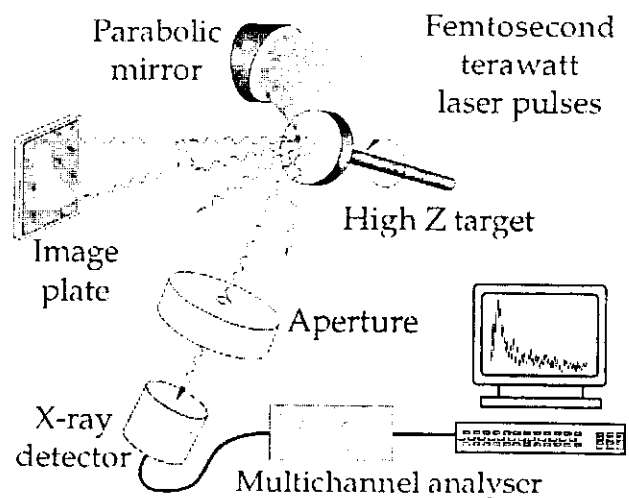

Fig. 12. Set-up for the production of laser-induced X-rays. (From Ref [13]).

Fig. 13. Single-shot X-ray recording of a human Incus bone and a metal mesh with a mesh site of 0.25 mm (from Ref. [27]).

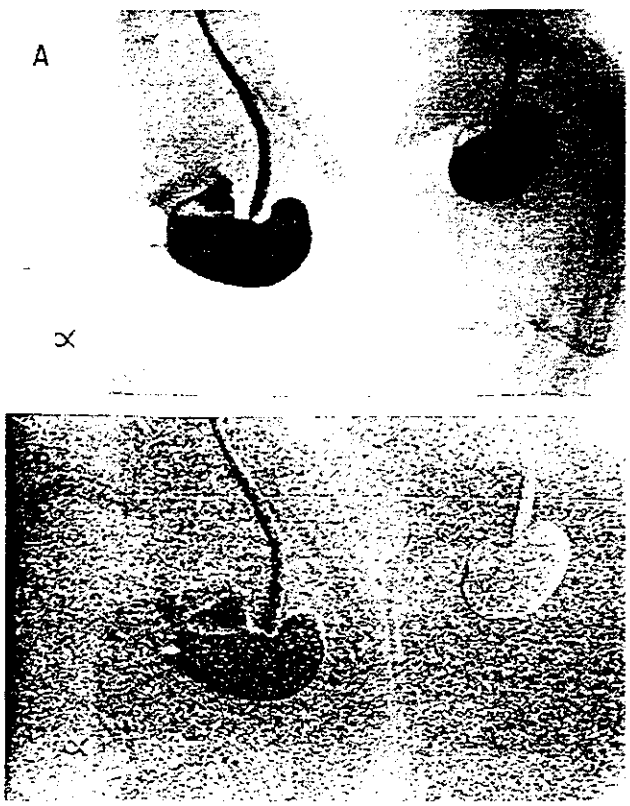

Fig. 14 Differential X-ray imaging of rats, for which solutions of gadolinium and cerium have been administered to the stomachs. (From Ref [13]).

the rat stomach to the right, containing gadolinium, appears brighter.

7. Discussion

The rapid development of more and more practical and cost-effective laser sources, detectors and computers facilitates the clinical implementation of laser technology. The non-invasive nature of the techniques and the real-time data acquisition are attractive features of the optical methods. Optical spectroscopy in principle allows molecular analysis, providing information not normally accessible with other modalities. For the future an increased use of combined diagnostic and therapeutic equipment can be anticipated. The field of lasers in medicine is very cross-disciplinary in nature, and fast progress will rely on an efficient collaboration between researcher of the medical, physical and chemical profession.

Acknowledgements

The author gratefully acknowledges a most fruitful collaboration with colleagues and graduate students at the Lund University Medical Laser Centre and with different European groups. This work was supported by the Swedish Engineering Science Research Council, the Swedish Board for Industrial and Technical Development, the Swedish Medical Research Council, the Swedish Cancer Society, The K. and A. Wallenberg Foundation, and the industrial partners Johnson & Johnson GmbH, Spectraphos AB and Xillix Technologies Corp.

References

1. Pettit, G. and Waynant, R. W. (Editors) "Lasers in Medicine" (Wiley, New York, in press).
2. Carruth, J. A. S. and McKenzie, A. L., "Medical Lasers Science and Clinical Practice" (Adam Hilger Ltd, Bristol 1986).
3. Tuchin, V. V., Laser Physics 3, 767 (1993).
4. Müller, G. and Roggan, A. (Editors) "Laser-induced Interstitial Thermotherapy" (SPIE, Bellingham 1996).
5. af Klinteberg, C., Svanberg, K. and Wang, I. (Editors) "Lund University Medical Laser Centre — Progress Report 1993–94/95" (Lund University, Lund 1996).
6. Marcus, S. L., in: "Photodynamic Therapy of Human Cancer: Clinical Status, Potential and Needs" (Edited by C. Gomer) (SPIE, Bellingham 1990), p. 1.
7. Pass, H. I., J. National Cancer Inst. **85**, 443 (1993).
8. Marcus, S. L., in: "Lasers in Medicine" (Edited by G. Pettit and R. W. Waynant) (Wiley, New York, 1995).
9. Svanberg, S., Physica Scripta **T26**, 90 (1989).
10. Svanberg, S., in: "Lasers in Medicine" (Edited by G. Pettit and R. W. Waynant) (Wiley, New York, in press), ch. 7.
11. Öberg. P. Å., Critical Reviews in Biomedical Engineering **18**, 125 (1990).
12. Müller, G. *et al.* (Editors) in: "Optical Tomography" (SPIE, Bellingham 1994).
13. Tillman, C., Mercer, I., Svanberg, S. and Herrlin, K., J. Opt. Soc. Amer. **13**, 209 (1996).
14. Kennedy, J. C., Potter, R. H. and Pross, D. C., J. Photochem. Photobiol. **6**, 143 (1990).
15. Svanberg, K., *et al.* Brit. J. Dermatology **130**, 743 (1994).
16. Andersson, P. S., Montán, S. and Svanberg, S., IEEE J. Quant. Electr. **23**, 1798 (1987).
17. Svanberg, K., *et al.*, Acta Radiologica (in press).
18. Svanberg, K. and Svanberg, S., La Recherche **24**, 686 (1993).
19. Aganauskiene, J., *et al.* "Characterization of myocardial tissue utilizing laser-induced fluorescence spectroscopy" (unpublished).

20. Alfano, R. R. *et al.*, Lasers Life Sci. **4**, 23 (1991)
21. Baraga, J. J., Feld, M. S. and Rava, R. P., Appl. Spectr. **46**, 187 (1992).
22. Andersson-Engels. S., Johansson, J. and Svanberg, S., Spectrochimchim. Acta **46A**, 1203 (1990).
23. Berg, R., Andersson-Engels, S. and Svanberg, S., in: "Optical Tomography" (SPIE, Bellingham 1994).
24. Berg, R., Jarlman, O. and Svanberg, S., Appl. Opt. **32**, 574 (1993).
25. Andersson-Engels, S., Berg, R. and Svanberg, S., J. Photochem. Photobiol. **16**, 155 (1992).
26. Herrlin, K., *et al.* Radiology **189**, 65 (1993).
27. Tillman, C., Persson, A., Wahlström, C.-G., Svanberg, S. and Herrlin, K., Appl. Phys. B **61**, 333 (1995).

Lasers in Medicine
Chapter 6

TISSUE DIAGNOSTICS USING LASERS

Sune Svanberg
Department of Physics, Lund Institute of Technology
P.O. Box 118
S-221 00 Lund, Sweden

Invited book chapter for

LASERS IN MEDICINE
G. Pettit and R.W. Waynant (Eds.)
Plenum, New York

(To Appear)

Abstract

Laser spectroscopic techniques are providing new possibilities for tissue diagnostics. Laser-induced fluorescence spectra for biological molecules have comparatively little structure, but sometimes have sufficient specificity to allow demarcation between diseased and surrounding normal tissue. This is particularly true if tumor marking has been performed with tumor-seeking agents, such as hematoporphyrin derivative (HPD) or δ-amino levulinic acid (ALA). Also atherosclerotically transformed vessel wall can be identified providing a means for spectroscopic guidance for angioplasty. Apart from time-integrated monitoring of the full fluorescence spectra, time-resolved data can be obtained for chosen fluorescence wavelengths to enhance demarcation capability. Raman spectra are much weaker but have a higher specificity, giving hope for future very selective optical biopsy sampling. Fluorescence instrumentation for point monitoring and imaging are described and examples from different clinical specialitites are given. Elastically scattered light can also be used for tissue analysis. Thus, tissue blood perfusion can be assessed by laser Doppler flowmetry, which now is also able to generate blood flow images. Photon migration studies in tissue constitute a strongly developing field. By time-resolved spectroscopy it is possible to follow the transport of photons through tissue. In particular, time-resolved transillumination with detection of only the first emerging photons allows enhanced viewing through tissue by reducing the image blurring due to light multiple scattering. Much research work is focussed on the development of mammography without employing ionizing radiation. Other aspects of photon migration in tissue are optical dosimetry for successful photodynamic treatment of malignant tumors and studies of brain oxygenation.

1. INTRODUCTION

While therapeutical aspects of lasers in medicine have been very dominant, tissue diagnostics techniques employing spectroscopy are now strongly emerging. Applications include endoscopic cancer detection using fluorescence, plaque monitoring in the circulatory system including coronary arteries, and tissue transillumination for optical mammography. Several factors contribute to the increasing interest for laser tissue diagnostics:

- Optical monitoring is non-intrusive in nature
- Non-ionizing radiation is employed
- Real-time data representation is possible
- Spectroscopy allows molecular specificity in analysis
- Point monitoring or imaging capability can be employed
- Integration of laser diagnostics and therapy is possible

Sometimes the term "optical biopsy" is used, which also gives the flavor of the attractive features of the new emerging methods. In comparison with well established diagnostic modalities such as X-ray radiography, NMR imaging, ultrasound imaging and positron emission tomography[1], the optical spectroscopic techniques are in an early stage of development. However, through extensive work at several research centers the optical techniques are swiftly developing, and clinically useful equipment is now becoming available.

The organization of the present chapter is as follows: Light interaction with tissue, forming the basis for optical tissue diagnosis, is reviewed in Sect. 2. In a following section, malignant-tumor diagnostics based on laser-induced fluorescence is treated, where point monitoring, multi-spectral imaging as well as time-resolved aspects are included. Monitoring of the interior of vessel walls and of the heart muscle is treated in Section 4, with a discussion of the possibilities of integration of diagnostics with a treatment modality. Finally, light scattering in tissue transillumination is treated in Section 5, which includes Doppler perfusion monitoring, optical dosimetry for photodynamic therapy and the detection of deep-lying malignant breast tumors using time-gated viewing. An outlook for the future concludes the chapter.

2. LIGHT INTERACTION WITH TISSUE

Optical diagnostics for medical purposes is based on the interaction of light with tissue. The interactions can be resonant or non-resonant in nature:

Resonant

Molecular absorption of laser light
Laser-induced tissue heating
Laser-induced photochemistry
Laser-induced fluorescence

Non-resonant

Elastic scattering
Raman scattering

Light/matter interaction mechanisms, spectroscopic instrumentation and measurement techniques are treated in text books on atomic and molecular spectroscopy, e.g. in Ref. 2. Here we will now discuss the different modes of interaction between light and tissue.

2.1 Molecular Absorption of Laser Light

When tissue is irradiated by laser light, a small fraction of the light is reflected but most of it penetrates into the tissue where it is either absorbed of scattered by the molecules. In certain wavelength regions absorption strongly dominates over scattering. The stronger the absorption, the smaller the penetration depth into the tissue will be. A schematic diagram of the absorption of some important biological constituents and chromophores, such as water, proteins, nucleic acids, haemoglobin and melanin is shown in Fig. 1[3]. Here also the emission wavelengths of some important medical lasers are included. As can be seen, water has two regions of strong absorption, one in the deep ultraviolet (UV) region and one in the infrared (IR) region. The absorption maximum in the case of the aromatic rings of proteins and the nucleic acids is in the UV region between 260 and 280 nm. Thus, in the UV region the laser light is highly absorbed by the water and the proteins in the tissue, resulting in a poor light penetration into the tissue. The same is true in the IR region starting at the second water absorption region for water at about 1.4 μm. Haemoglobin in the blood absorbs light in a broad wavelength region up to red light (about 600 nm) with a pronounced absorption maximum at about 400 nm and additional weaker peaks in the green/yellow region. Above 600 nm the absorption of blood is weak. Melanin, the most important chromophore in the epidermis, absorbs light in a region from UV to near IR. Between 600 nm and 1.3 μm the attenuation coefficients of the tissue molecules are comparatively small, resulting in a wavelength region with favourable light penetration properties, with increasing penetration towards the IR region. Considering the total tissue absorption, it can be noted that the human body is as transparent as can be in the region 1.0 - 1.3 μm.

The absorptive properties of a surface can also be monitored indirectly in reflectance. This is a well-known phenomenon forming the basis for the human perception of colors. E.g., the red color of blood can be understood from the absorption curve given in Fig. 1, where all colors below 600 nm in the impinging white light are strongly absorbed by the haemoglobin molecules. Red light, however, is not absorbed but can be scattered, reaching the eye of the observer. In the practice, reflectance spectroscopy performed by the doctor's eye and coupled to the processing of an experienced brain is a most important means in assessing human tissue status. The technique can be refined by using a spectrometer also giving access to the IR region, where characteristic absorption bands due to molecular vibrational transitions modify the impinging radiation. This technique can basically yield the same type of information as Raman spectroscopy, discussed below. Analysis of reflected light forms the basis for global earth-resource monitoring using passive satellite sensors[4].

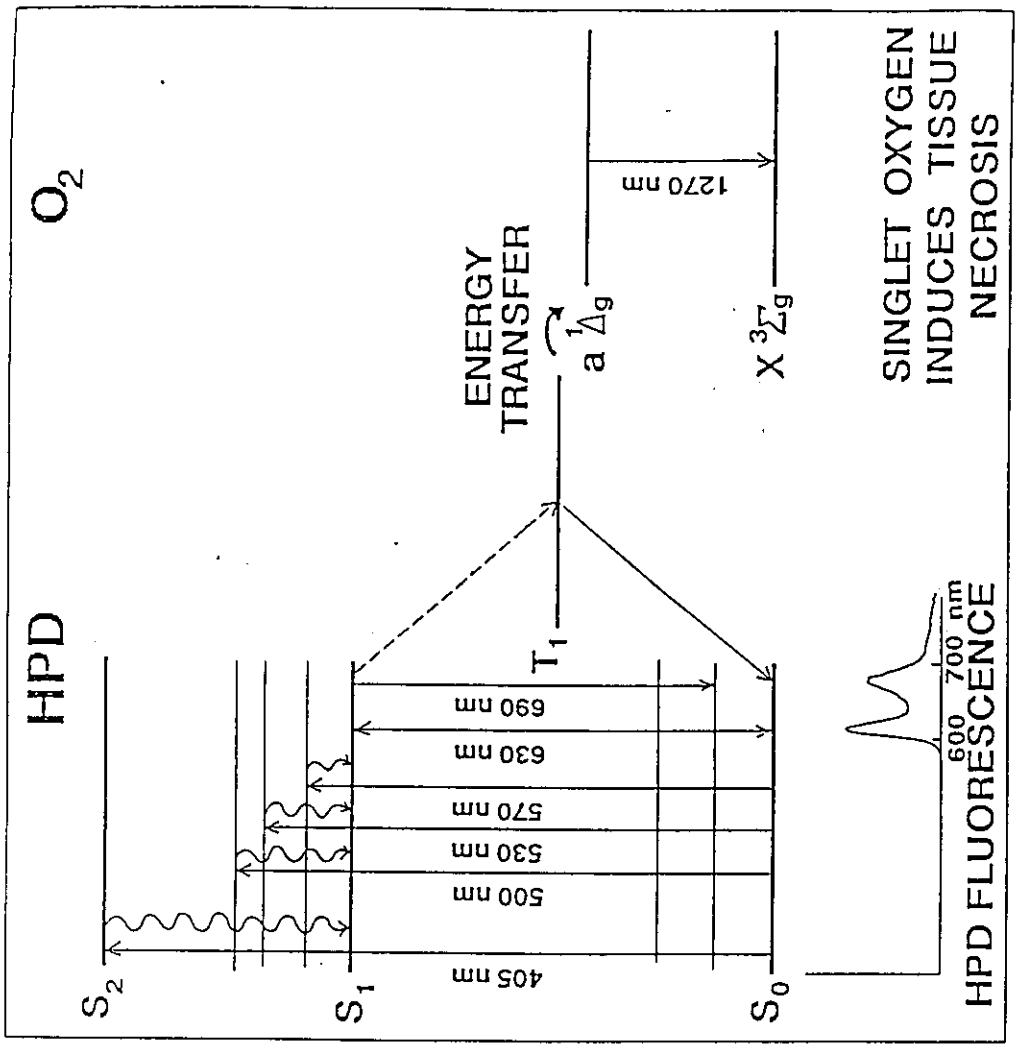

Figure 2.

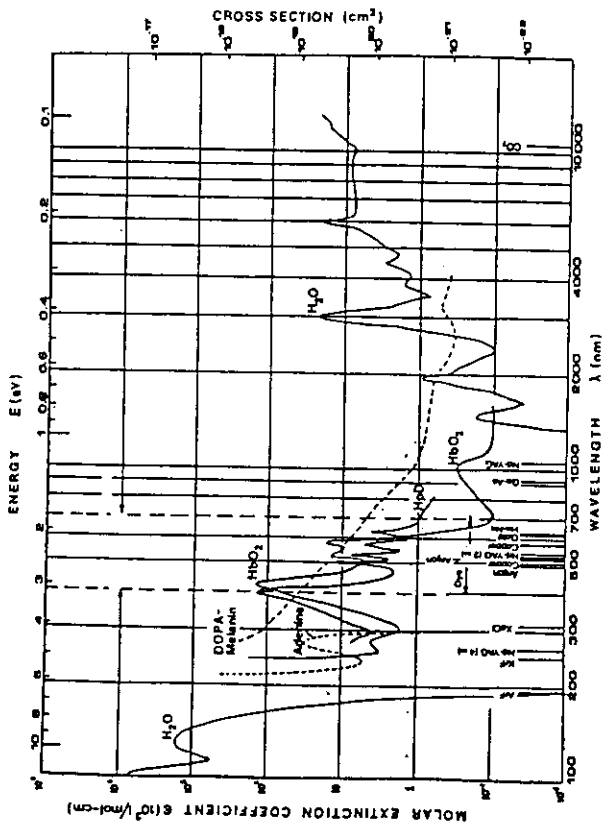

Figure 1.

2.2. Laser-Induced Tissue Heating

Laser-induced tissue heating occurs through the conversion of electromagnetic energy into thermal energy. This photothermal process occurs when biomolecules have absorbed light quanta to arrive in an excited state and return non-radiatively to lower excited levels, transferring their energy to the tissue. In the thermal mode of tissue interaction the choice of wavelength, as well as the tissue type, determine the light penetration depth. Heating leads to protein coagulation (60°C), body fluid boiling (100 °C) and tissue carbonisation (200 °C) that can be used for haemostasis and tissue surgery. This is a major application of lasers in medicine, having much impact in ophthalmology, dermatology and general surgery. The carbon dioxide laser (10.6 μm) has a very low tissue penetration due to water absorption, as has the argon-ion laser (488, 515 nm), due to haemoglobin. If a dye laser is tuned to 580 nm it can be made to quite selectively be absorbed by the haemoglobin in small vessels (see Fig. 1). Thus, haemangioma, such as portwine stains, can be efficiently treated while sparing surrounding, normal tissue. Maximum penetration occurs for the Nd:YAG laser (1.06 μm), which induces wide coagulation zones around surgical cuts. The various clinical applications of lasers operating in the thermal mode are discussed in many chapters of this book. For the purpose of tissue diagnostics using laser techniques thermal effects should be avoided by keeping the laser fluence sufficiently low. We only include this brief discussion of laser thermal interaction in order to clarify the limitations of optical tissue diagnostics.

For UV wavelengths the penetration depth of laser light is only of the order of 1-100 μm. Such radiation can be used to induce fluorescence in the biomolecules, which provides an important means of tissue diagnostics. However, high incident fluences of such radiation in short pulses leads to explosive tissue ablation, and must thus be avoided in all diagnostic work. Laser tissue ablation, on the other hand, has important medical applications for myopia correction by corneal reshaping and as a modality for clearing occluded vessels using transluminal optical fibres, as discussed in Chapters 10[5] and 11[6].

2.3 Laser-Induced Photochemistry

Optically excited molecules can, instead of releasing their excess energy as heat, transfer their energy to other molecules inducing chemical reactions of therapeutic interest. Optical treatment of psoriasis patients, or new-born infants with an excess of bilirubin, are well-known examples of medical photochemistry. Photodynamic tumor therapy (PDT) using tumor-seeking agents is a further example of special interest in our context. The most commonly used tumor sensitizer is haematoporphyrin derivative (HPD), which is commercially available under the trade name of Photofrin.

The absorption curve of HPD is included in Fig. 1. When injected intravenously such molecules are selectively retained to a higher degree in malignant tumor tissue compared to other surrounding tissue. It can be noted in the figure that the absorption maximum of HPD is around 400 nm like for haemoglobin in the blood, but also that HPD exhibits four more absorbing peaks with the last one at 630 nm, where blood absorption is strongly reduced. Therefore, laser light of 630 nm instead of 400 nm is used, in order to penetrate deeper into the tumor tissue.

A schematic diagram showing the energy levels of the HPD molecule with absorption and fluorescence emission wavelengths is shown in Fig. 2[7]. Following light irradiation, HPD molecules become excited. The molecules can then be deexcited following two main pathways. In the first one, the molecules non-radiatively are transferred to the bottom of the first excited band, from where a radiative decay follows with the emission of a dual-peaked fluorescence light distribution in the red spectral region. This emission can be used for the diagnostics of malignant tumors, since the characteristic red fluorescence only follows from irradiated tissue that has retained the HPD molecules. This diagnostic aspect will be discussed extensively in the next sub-section. In a second deexcitation pathway the molecules are transferred into the triplet state. From here the excitation energy can be transferred to ground-state tissue oxygen molecules that are excited into their singlet state. Singlet state oxygen is known to be an extremely toxic agent for living cells. As the HPD in the cells mediates this energy transfer, which results in singlet-oxygen formation, the cells are transformed from viable malignant cells to non-viable necrotic cells. This is the essence of photodynamic therapy, that is now being pursued on an experimental basis at many centers throughout the world. The therapeutic aspect as well as the diagnostic one are schematically illustrated in Fig. 3[7]. Reviews of clinical PDT have been given in Refs 8,9. The field is further treated in Chapter 15 of this volume[10].

2.4 Laser-Induced Fluorescence

Laser-excited molecules have a probability to return to the ground-state by emitting fluorescence light. Fluorescence spectroscopy is treated in detail, e.g. in Refs 11,12. The fluorescence always occurs for longer wavelengths (Stokes shift). For large biomolecules the fluorescence normally exhibits a rather structure-less intensity distribution as a function of wavelength, reflecting the distribution of substates in the ground electronic level. However, by choosing the excitation wavelength properly and accurately analysing the fluorescence light distribution, it is frequently possible to obtain diagnostic information for the tissue molecules. Using short-pulse excitation, it is also possible to measure the decay time for the fluorescence light yielding additional information. Many

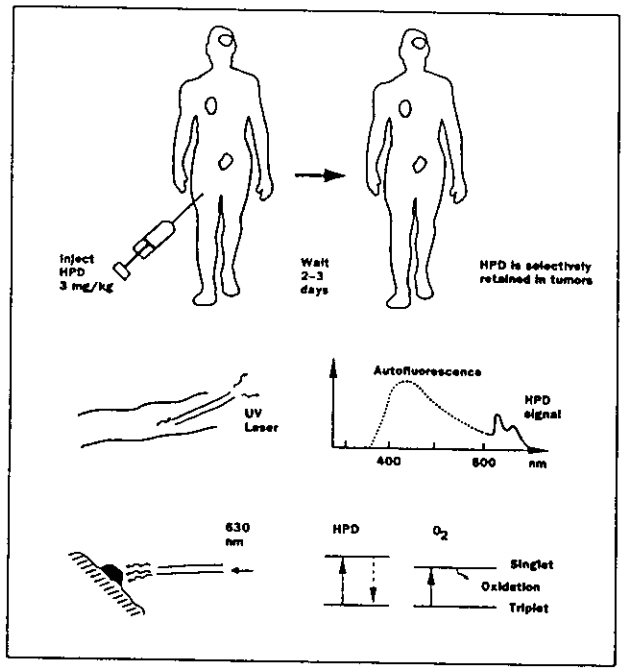

Figure 3.

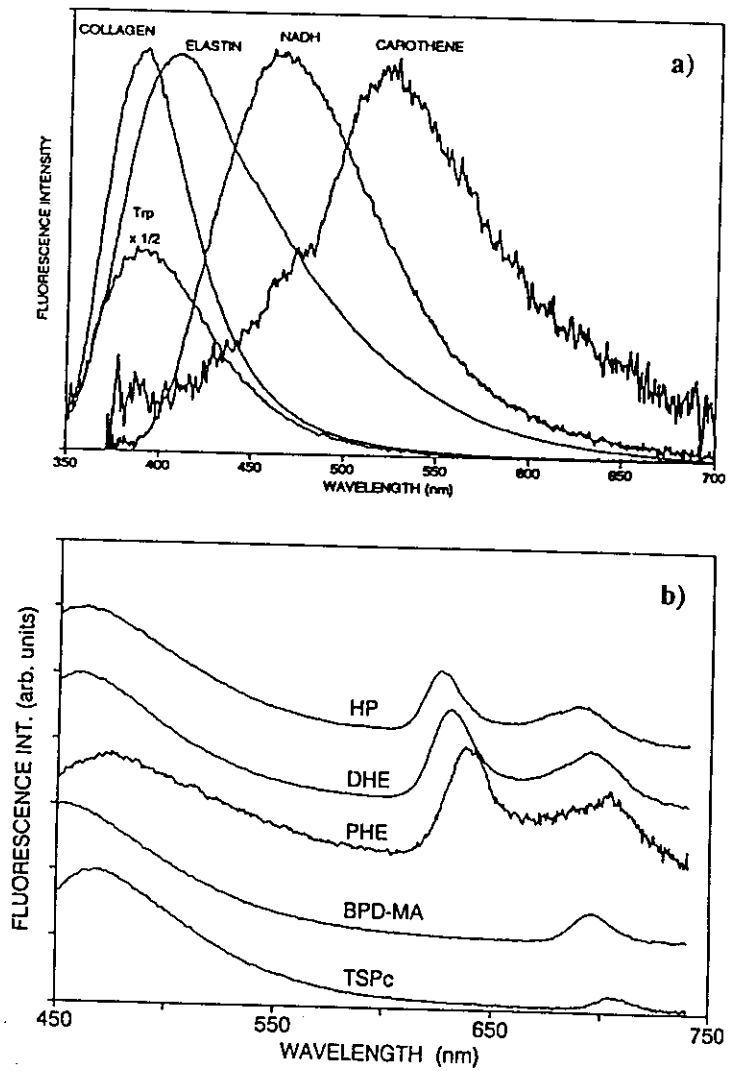

Figure 4

different chromophores may contribute to the tissue signal: endogenous molecules such as NADH, NAD^+, collagen and elastin giving rise to so called auto-fluorescence, and added, tumor-seeking agents such as haematoporphyrin derivative, phtalocyanines and chlorins, all featuring sharp and characteristic signals in the red and near-IR region. Examples of fluorescence spectra for different pure tissue substances and of tumor-seeking agents, injected in the same type of tumor-bearing rats, are shown in Fig. 4[13,14].

2.5 Elastic Scattering

Light scattering in tissue is important for red and near-IR light, which is not strongly absorbed by the tissue constituents. The scattering is normally elastic, i.e. no change in wavelength occurs. If absorption is low, many scattering processes may occur in a more or less random way before the photon is ultimately absorbed or escapes out from the tissue. The fate of an individual photon is determined in a complex interplay between scattering and absorption. The process can for certain geometries be described by solving the diffusion equation, specifying values for the absorption and scattering coefficients μ_a and μ_s, respectively. Of special interest is to study the case of transillumination through a thick tissue sample (few cm). Many of the photons have been scattered a multitude of times resulting in effective pathlengths of tens of centimeters. If large computer capacity is available, the photon propagation can be simulated using Monte Carlo techniques, where photon trajectories are followed for a large number of events to build up an intensity distribution. In such calculations the mean cosine value between the incoming and scattered photon directions of propagation is also included (Refs 15-19).

The presence of scattering makes tissue absorption measurements much more involved as discussed above. The path-length in tissue that has been traversed cannot be assessed in steady-state measurements, making a direct use of the Beer-Lambert absorption relation impossible. Time-resolved monitoring of picosecond pulses, on the other hand, allow well-defined such measurements, that are of particular interest for measuring tissue oxygenation, using absorptive spectral features in the red/near-IR region as shown for oxygenated haemoglobin in Fig. 1. De-oxygenated haemoglobin has a different spectral structure.

If light is scattered against a moving particle a very small frequency shift, proportional to the in-line velocity occurs due to the Doppler effect. The only important moving particles in the body are the red blood cells. In the superficial capillary vascular bed accessible for non-intrusive light scattering measurements, the flow velocities are low, typically 1 mm/s. For the helium-neon laser wavelength (633 nm) this corresponds to a frequency shift of only about 3 kHz out of about 5×10^{14} Hz. Measurements of such small shifts can be accomplished by a heterodyne technique, where the beat frequency between the frequency-shifted light and the unshifted light, scattered from the fixed cell structures is observed. Since the scattering geometry is undefined, an average of different flow velocities and flow directions is obtained yielding an effective signal, which is related to the superficial blood perfusion of the investigated tissue. Laser Doppler techniques for tissue perfusion measurements are treated in Refs 20,21.

2.6. Raman Scattering

Raman scattering is inelastic, leading to scattered photons of strongly changed wavelength. It may be seen as an excitation to a virtual (non-resonant) state and an immediate transfer from this state to a lower-state of different energy than that of the initial state. In cases of medical interest the lower state splittings are due to vibrational energy. The resulting shifts are characteristic for vibrations in specific molecular groups. Although Raman scattering provides a much higher molecular specificity than laser-induced fluorescence, there is a sensitivity problem, since Raman scattering is many orders of magnitude weaker than laser-induced fluorescence. Thus, unless proper precautions are taken the signals tend to be swamped by the fluorescence signals.

3. SPECTROSCOPIC DIAGNOSTICS OF MALIGNANT TUMORS

3.1 Basic Considerations

In this section we will focus on tumor diagnostics using laser-induced fluorescence and will only briefly comment on Raman spectroscopy, which is presently less developed. At first glance it might seem as a formidable task to derive any information from tissue fluorescence considering the many types of complex organic molecules that form up living tissue. We will first present typical tissue spectra in Fig. 5[22,23] and discuss the type of information it is containing. The sample chosen is a rat tumor in a muscle environment[24] and we show spectra for tumor as well as for surrounding normal tissue and for two excitation wavelengths, 337 and 405 nm. The rat had been injected by a dose of haematoporphyrin derivative (Photofrin) 2 days earlier. For both excitation wavelengths a broad intensity distribution extending from the blue to the near IR region is obtained. In the measurements the strong elastically scattered light from the primary laser excitation light is suppressed by a suitable filter, blocking completely towards shorter wavelengths but letting all longer wavelengths through, basically unattenuated.

In the tumor spectra we can see the characteristic dual-peaked fluorescence signal from HPD in the red wavelength region (cf. Figs 2 and 4). This signal is less prominent in the normal tissue due to the selective retention of the drug in tumor tissue. The signal in the blue-green region is called the *autofluorescence*, since it is due to the natural chromophores in the tissue. This signal is peaking at about 470 nm. The blue-green fluorescence is much stronger and the red HPD signal much weaker when 337 nm is chosen as the excitation wavelength. This can be understood from the absorption curves in Fig. 1. 405 nm corresponds to the absorption maximum (the Soret band) of the HPD molecules, and excitation here is more efficient than at 337 nm. Many chromophores contribute to the signal in the blue-green wavelength region (Examples are given in Fig. 4a). The absorption for most of these molecules increases for shorter wavelengths. An interesting observation relating to Fig. 5 is that the intensity of the blue-green signal is reduced in tumor tissue as compared to normal one. This was noted already in 1984[25] and seems to primarily be due to a transformation of strongly fluorescing NADH in normal tissue to NAD^+ with a much weaker fluorescence[26-28]. These observations form the basis for efficient tumor detection and demarcation using laser-induced fluorescence after injection of a tumor-seeking drug: the red fluorescence increases and the blue-green fluorescence decreases in a tumor. Both effects can be utilised in a convenient way by

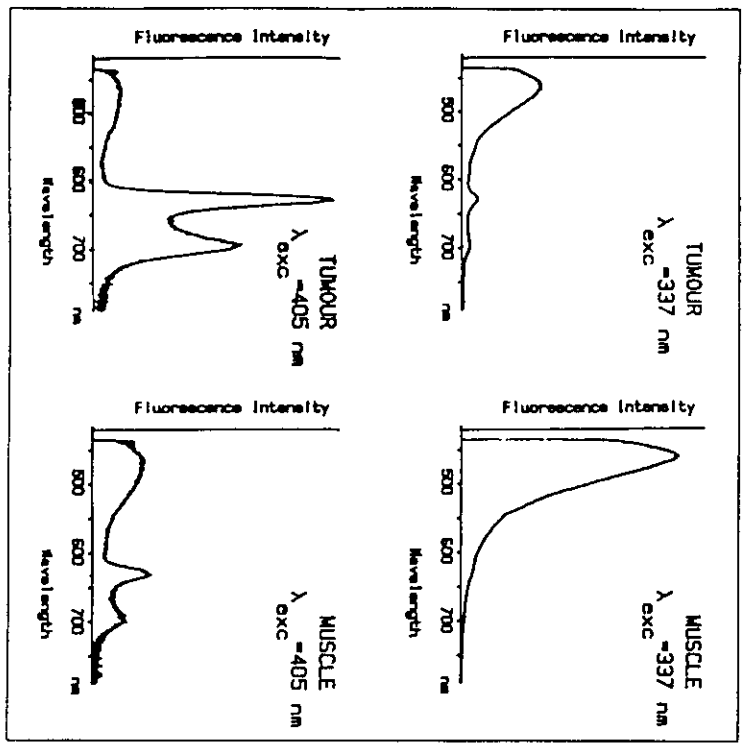
Fluorescence Intensity
Wavelength
TUMOUR
λ exc =405 nm
Fluorescence Intensity
Wavelength
TUMOUR
λ exc =337 nm
Fluorescence Intensity
Wavelength
MUSCLE
λ exc =405 nm
Fluorescence Intensity
Wavelength
MUSCLE
λ exc =337 nm

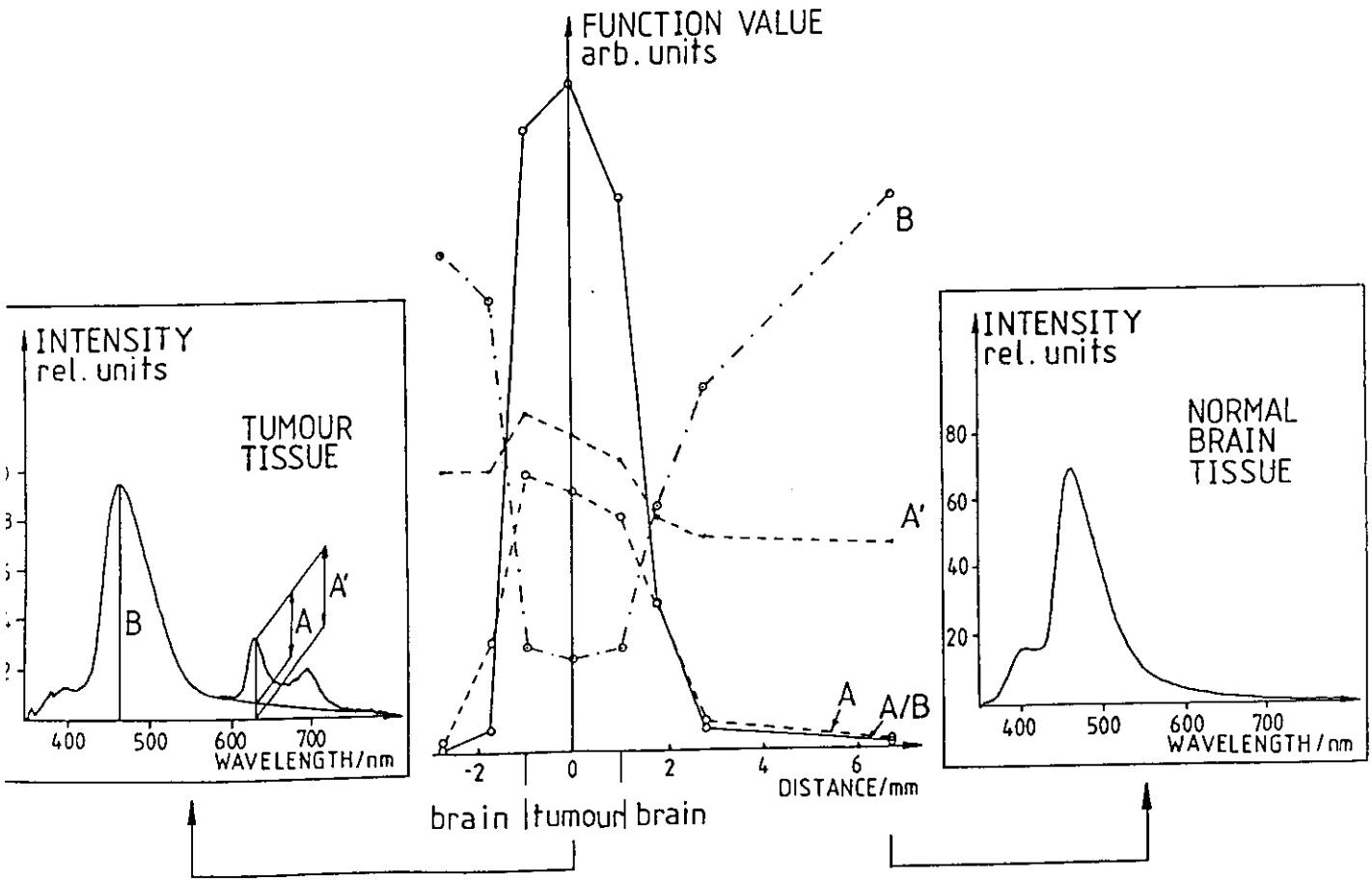
INTENSITY
rel. units
TUMOUR
TISSUE
B
A
A'
400
500
600
700
WAVELENGTH/nm
FUNCTION VALUE
arb. units
B
A'
A
A/B
-2
0
2
4
6
DISTANCE/mm
brain
tumour
brain
INTENSITY
rel. units
NORMAL
BRAIN
TISSUE
80
60
40
20
400
500
600
700
WAVELENGTH/nm

dividing the red signal intensity by the blue intensity[25,29]. This is illustrated in Fig. 6[30] for the case of a scan through a tumor, inoculated in a rat brain. The rat had been injected with Photofrin (1 mg/kg bodyweight) 24 hours before the animal was sacrificed and the fluorescence investigation was performed. Typical spectra for normal and tumor regions are included in the figure, with the red intensity at 630 nm denoted by A´ and the blue intensity at 470 denoted by B. The background-free HPD signal at 630 nm is denoted by A. In the scan the red increase and the blue decrease in the tumor are very evident. Contrast enhancement is obtained by forming the ratio A/B. The use of such a dimensionless ratio also has other important advantages, particularly in practical clinical work, since dimensionless quantities are immune to

* distance changes between tissue and measurement equipment
* variations in angle of incidence of radiation on tissue
* fluctuations in illumination source and detection system efficiency.

The ratio signal is basically only sensitive to the intrinsic properties of the tissue. If the drug-related signal is weak and sitting on a substantial slope of autofluorescence intensity, it is important to use the background-free signal intensity, not to loose contrast.

3.2 Instrumentation for Point Monitoring of Laser-Induced Fluorescence

In this section we will present equipment suitable for fluorescence studies of tissue. A sealed-off nitrogen laser, emitting at 337 nm, is a very convenient excitation source. This laser typically generates 3 ns long pulses at 10 Hz, and can also be employed to pump a compact dye laser, converting the pump radiation to a longer, selectable wavelength. This is the excitation source used in the recording of the data in Figs 5 and 6. Fluorescence is best analysed with an optical multichannel analyser system consisting of a spectrometer equipped with an intensified diode-array detector in the focal plane. For each exciting laser pulse the whole fluorescence spectrum is captured and can be directly displayed on a monitor and stored in a computer. The image intensifier, providing amplification of the weak light signals, is gated synchronously with the laser pulses. In this way background radiation due to day-light of operation lamps can be suppressed in the recordings.

In laboratory investigations the excitation light can be directed to the sample by means of mirrors and the resulting fluorescence light can be collected by an optical set-up of mirrors and lenses. The fluorescence light thus captured can be directed onto the entrance slit of the spectrometer. However, for clinical measurements a more flexible fluorosensor is needed. Such an instrumentation is shown in Fig. 7[31]. The excitation laser light from the laser is focused into an optical fiber which can be sterilised when used in surgical procedures or used through the biopsy channel of an endoscope. The fluorescence light is captured through the same fiber separated from the excitation light by a dichroic mirror. The fluorescence light is focused onto the slit of a multichannel analyser system. The fluorosensor is constructed as a mobile system and can easily be transported between different clinics. Two systems of this construction are used for fluorescence studies at various clinics at the Lund University Medical Laser Center. A photograph of such a system is shown in Fig. 8. Most of the examples of fluorescence spectra shown in this chapter have been recorded with this type of equipment.

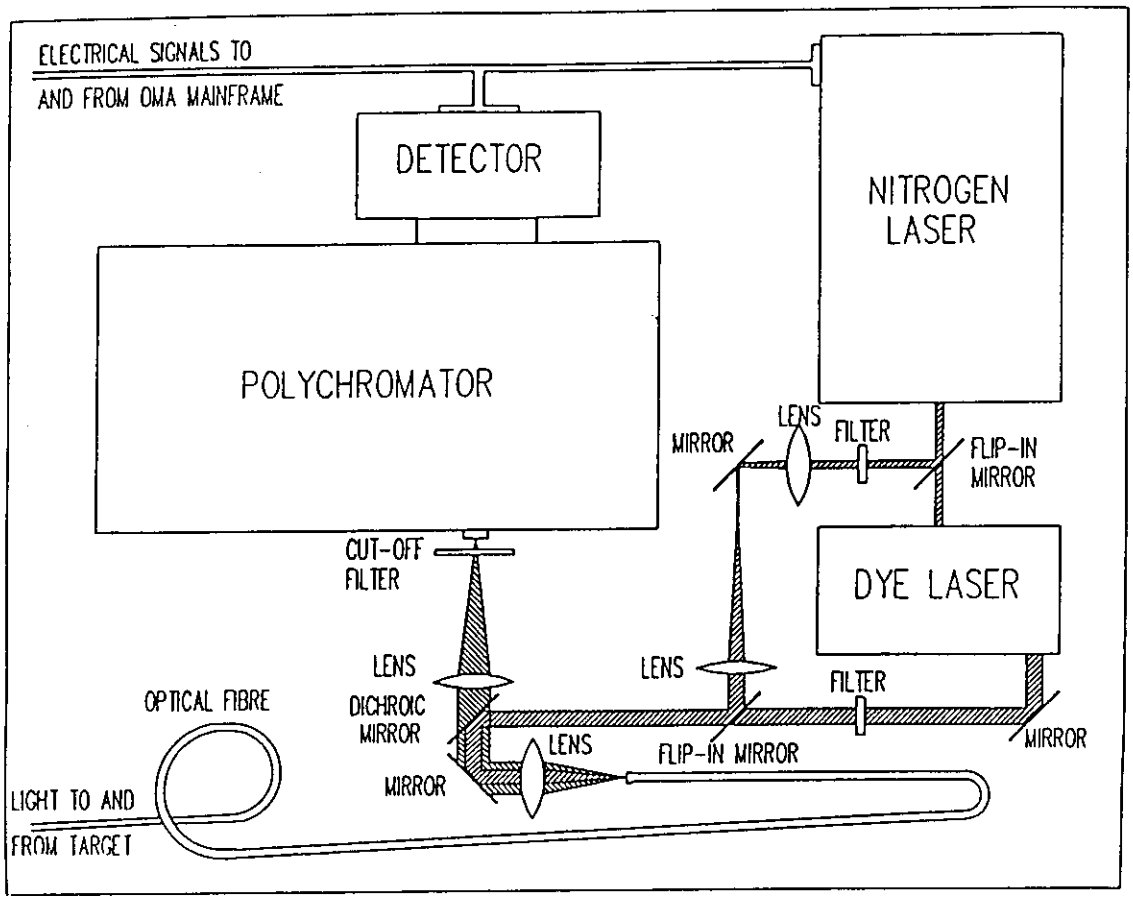
ELECTRICAL SIGNALS TO
AND FROM OMA MAINFRAME
DETECTOR
NITROGEN LASER
POLYCHROMATOR
MIRROR
LENS
FILTER
FLIP-IN MIRROR
CUT-OFF FILTER
DYE LASER
LENS
LENS
FILTER
OPTICAL FIBRE
DICHROIC MIRROR
LENS
FLIP-IN MIRROR
MIRROR
MIRROR
LIGHT TO AND
FROM TARGET

Interference filters can also be used to select the interesting wavelengths for fluorescence signal detection. The fluorescence light can then be divided by dichroic beamsplitters and directed towards individual photomultipliers. One detection channel can be centered at the 630 nm peak while another one is set at 470 nm. An additional channel can be centered at 600 nm to provide a signal for background subtraction. Gated integrators are used to capture the signal during a brief time interval, followed by signal processing to provide the desired ratio signal.

It is also possible to use a mercury lamp as an excitation source instead of a laser. Such a system is described in Ref. 32, and was further developed and tested as described in Ref. 33. A chopper wheel equipped with interference filters analyses the fluorescence light beam and filters out two excitation wavelengths, i.e. 365 and 405 nm. The filtered light is reflected by a dichroic beam splitter and is focused into the investigation fiber. The fluorescence light comes back through the fiber. Here interference filters sequentially select the useful wavelengths, i.e. 470, 600 and 630 nm for both excitation wavelengths in cases of tumor diagnostics utilising HPD sensitisation. The light is recorded by a photomultiplier tube and the signal is electronically integrated during the passage of every filter. The result is digitised and fed to a computer. In this way three fluorescence wavelengths can be investigated at two excitation wavelengths for every tissue spot under study.

3.3 Point Monitoring of Cancer using Laser-Induced Fluorescence

In this section we will give some examples of point monitoring of fluorescence related to malignant tumor detection. Data for human superficial tumors are shown in Fig. 9[34,35]. In the left part of the figure fluorescence spectra and evaluated data from a scan are shown for a basal cell cancer in a patient, that was injected by 2 mg/kg body weight of Photofrin 3 days before the fluorescence measurements. In the right part of the figure data for a breast carcinoma metastasis are shown in a similar way. This patient was studied 1 day after the same dose of Photofrin. A good demarcation of the tumor is obtained for both tumors, particularly in the A/B signal.

Extensive measurements on low-dose injected bladder cancer patients were made at the Department of Urology, University of Leuven[33]. The patients were injected by 0.35 or 0.50 mg/kg bodyweight, which is a low enough dose do avoid sun sensitisation, which at therapeutic dose injection (=2 mg/kg bodyweight) requires that patients be kept at reduced light level for about 4-6 weeks. Spectra for a papillary bladder tumor are shown in Fig. 10 for 337 and 405 nm excitation. It can be seen, that there is a very strong reduction in the blue-green fluorescence for tumor tissue, and also a prominent change in the spectral shape when 337 nm is employed. This change allows malignant tumor detection without using the HPD signal, which only appears clearly for 405 nm excitation, optimising the conditions for HPD detection, while at the same time reducing the autofluorescence intensity. Clinically, the most important task is to be able to identify dysplasia and carcinoma *in situ*, and it was shown, that such tissue has sufficiently different spectral characteristics to be distinguished from normal tissue. Spectral curves for mild and severe dysplasia are included in Fig. 10. Data for tissues from 21 patients are shown in Fig. 11. Fluorescence monitoring on tumors of the prostatic gland have also been performed after low-dose Photofrin injection and surgical resection. As can be seen

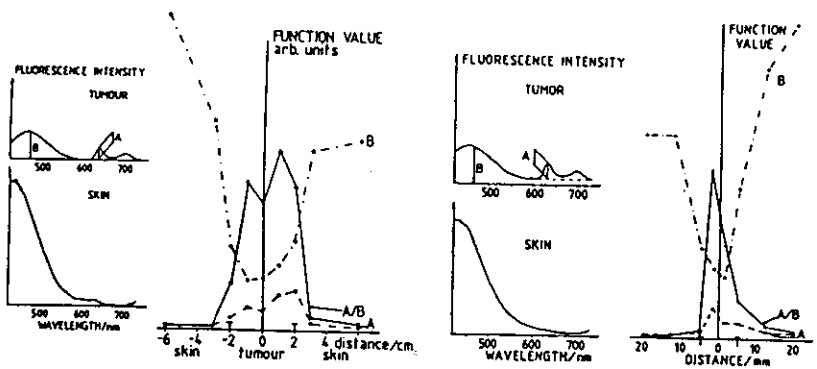

Figure 9.

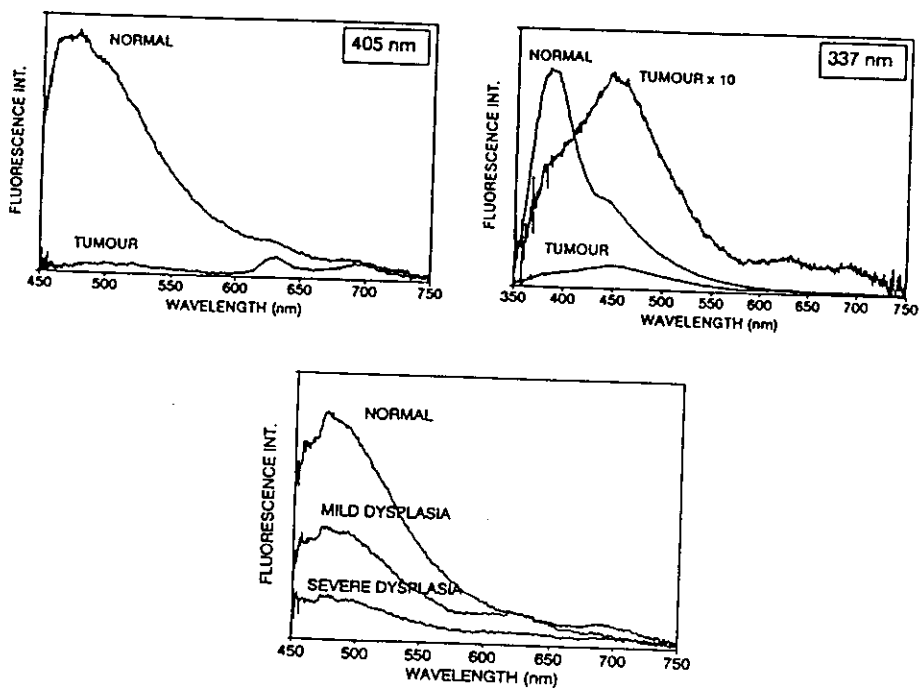

Figure 10.

Figure 12.

Figure 11.

in Fig. 12, tumors are characterised by an increase in the red fluorescence and a decrease in the blue-green fluorescence[36,37].

The lung is, like the bladder, an important location where early tumor detection can have a major influence on the course of the disease. This is particularly true for patients with a positive sputum test but negative biopsy sampling. We have studied the spectral characteristics of lung tissue during bronchoscopy with regard to autofluorescence[31] and after Photofrin injection[36,38]. Spectra for a low-dose injected patient are shown in Fig. 13[38].

Tissue diagnostics based on fluorescence can sometimes be performed without any injection of a drug, utilising the properties of endogenous chromophores only. Early such work was performed by Chinese researchers (see, e.g. 39,40), particularly regarding the gastro-intestinal tract, in which endogenous porphyrins frequently localise in tumors. However, endogenous fluorescence can also be utilised to detect lung and colon tumors, and also malignancies at many other locations[41-45].

Unwanted side-effects of skin sensitisation can be avoided by using topical application in the case of superficial tumors instead of systemic injection of a sensitising drug. Topically applied δ-amino levulinic acid (ALA) can be used for PDT of superficial skin tumors[46]. ALA penetrates the damaged keratin in the dermis but not the undamaged parts. ALA is a precursor in the biosynthetic pathway of the blood pigment haemoglobin. ALA is a non-photoactive substance, but within the haem cycle it is transformed into protoporphyrin, which is a photodynamically very potent agent. This process is illustrated in Fig. 14[47]. The steps from ALA to protoporphyrin appear comparatively fast, while the last step to haemoglobin is relatively slow. Thus, an accumulation of protoporphyrin can be induced in the tumor cells. Subsequent exposure to photoactivating light leads to a selective destruction of the lesions. In a first publication a 90% response rate for basal cell carcinoma following a single treatment was found[46]. We have reported the same response rate for different kinds of superficial skin tumors, including basal cell- and squamous cell carcinoma[47]. The conversion of ALA into protoporphyrin in tumors can be readily followed using laser-induced fluorescence[47,48]. The superior tumor demarcation properties of ALA are illustrated in Fig. 15[47-49] for the case of a human basalioma. In the lower part of the figure the corresponding fluorescence signals after PDT (60 J/cm^2) are shown. A strong photo-bleaching of the drug occurs, which can be used for dosimetry to ascertain that the correct light dose has been delivered to all parts of the tumor[48]. The bleaching of the drug in the upper, strongly exposed tissue layer also allows a more efficient treatment of deeper laying layers by continued light irradiation, since the upper layer cannot be overtreated[50].

As already mentioned there is an ongoing search for even better sensitizers, frequently concentrating on the behaviour in PDT procedures. Most sensitizers simultaneously have fluorescence properties that are useful for tumor demarcation. A list of new sensitizers with wavelengths for PDT excitation and fluorescence detection is given in Table 1.

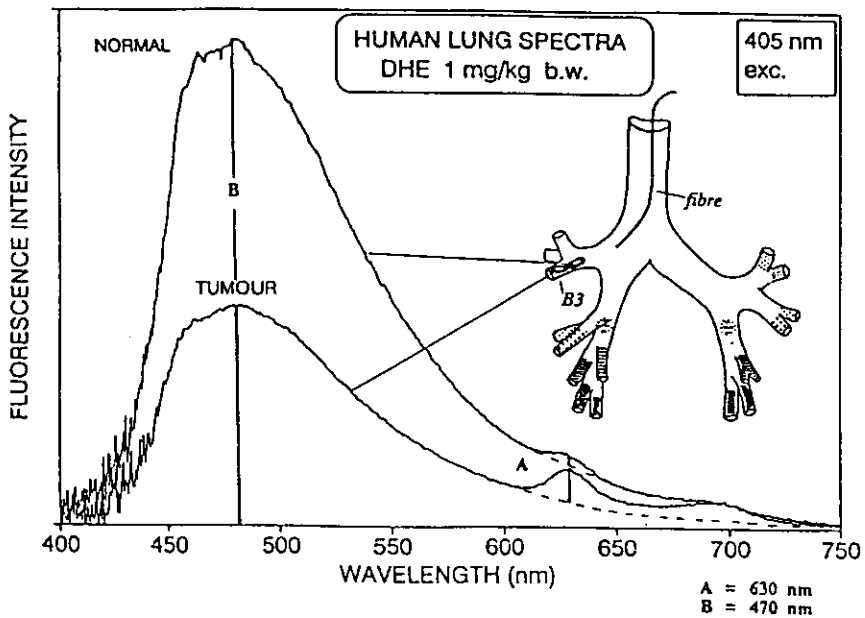

Figure 13.

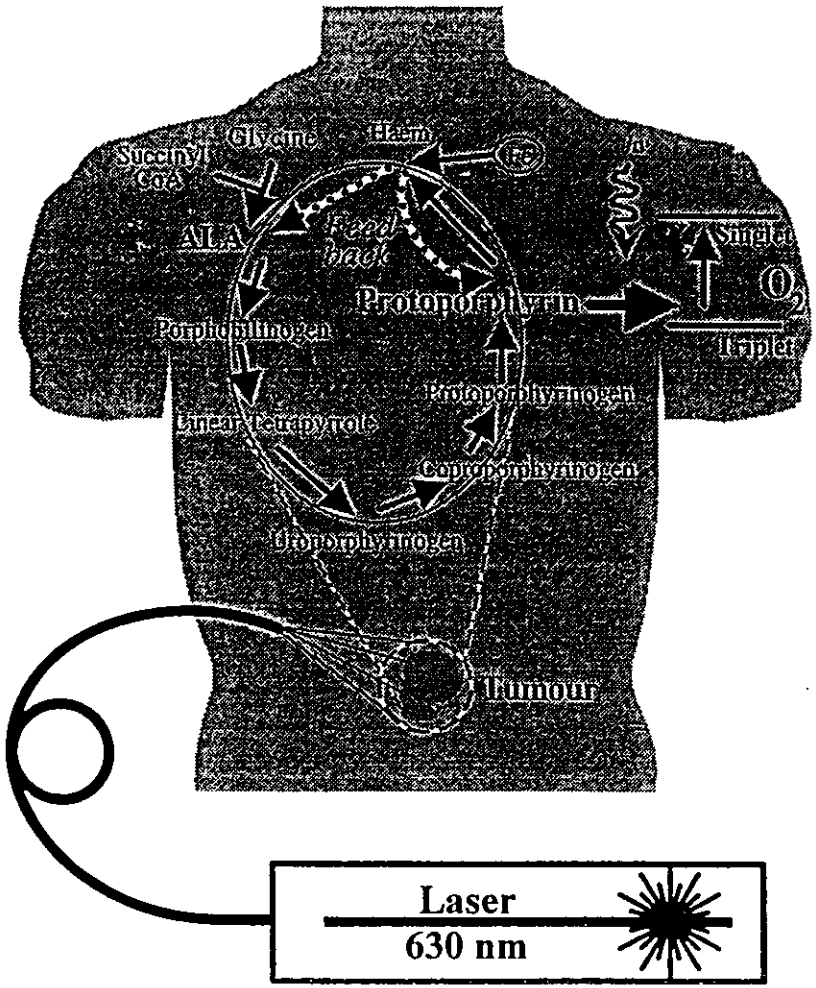

Figure 14.

3.4 Equipment for Imaging

It is of great diagnostic interest to extend fluorescence monitoring with incorporation of the contrast-enhancement techniques illustrated in Figs 6 and 11 into imaging measurements. This has been accomplished in our group, which has developed a multi-color fluorescence imaging system, starting with a one-dimensional proof-of-principle demonstration[51] later extended into full two-dimensional imaging[52-56]. In order to simultaneously obtain spatial and spectral resolution, the fluorescence light is divided using a multi-mirror arrangement as illustrated in Fig. 16. By using a spherical mirror which is divided into four individually adjustable sectors, four identical images can be sent to an intensified matrix detector, a CCD camera. By placing optical filters in front off the different mirror sectors, fluorescence images in selected colors are obtained simultaneously. In the four different images computerised calculations of dimensionless function values can be performed for each spatial location of the tissue investigated and a generalised image in an optimised contrast function can be produced. This function would normally be the ratio between the background-free 630 nm peak intensity A and the blue-green intensity B at about 470 nm. A properly weighted recording at 600 nm (kD) provides the background intensity. The weighting factor k also takes differences in optical efficiency into account and is adjusted to result in a zero intensity value for A= (A´-kD) when no tumor is present. A photograph of a fully clinically adapted fluorescence imaging system based on the principles given here is shown in Fig. 17. This system can be used together with endoscopes of different types allowing, e.g. lung and bladder investigations.

3.5 Multi-Color Fluorescence Imaging of Tumors

Fluorescence images at 630, 600 and 470 nm are shown in Fig. 18[55] for a human T-cell lymphoma tumor. Also included is the resulting image using the contrast function (A´-kD)/B, showing the tumor with a very clear demarcation towards surrounding normal tissue. An nitrogen-laser-pumped dye laser was employed for fluorescence excitation. The data were obtained with a laboratory instrumentation requiring substantial processing time to produce the final image. In an industrial prototype, a considerably higher processing rate was achieved using a vector processor for image processing. Up to eight images/s could be obtained allowing basically "live" recording of tumors. An example of a processed image from that system is shown in Fig. 19[55]. This is a direct photograph of the monitor screen, showing a rat tumor, in an animal that had been injected with Photofrin at a concentration of 15 mg/kg bodyweight. Registrations of a basal cell cancer and a benign naevus in a patient subjected to topically applied ALA, using the system shown in Fig. 17, are given in the left part of Fig. 20[56]. The upper image is a normal color registration of the investigated area. In the lower image the processed, thresholded and color-coded cancer contrast functional image has been added to the normal color image using a video mixer. It can clearly be seen how the basal cell carcinoma is identified as a malignant lesion while the naevus is left unmarked. To the right in the same figure corresponding images for a squamous cell carcinoma of the vocal cord are shown. Further fluorescence imaging systems are described in Refs 57-60.

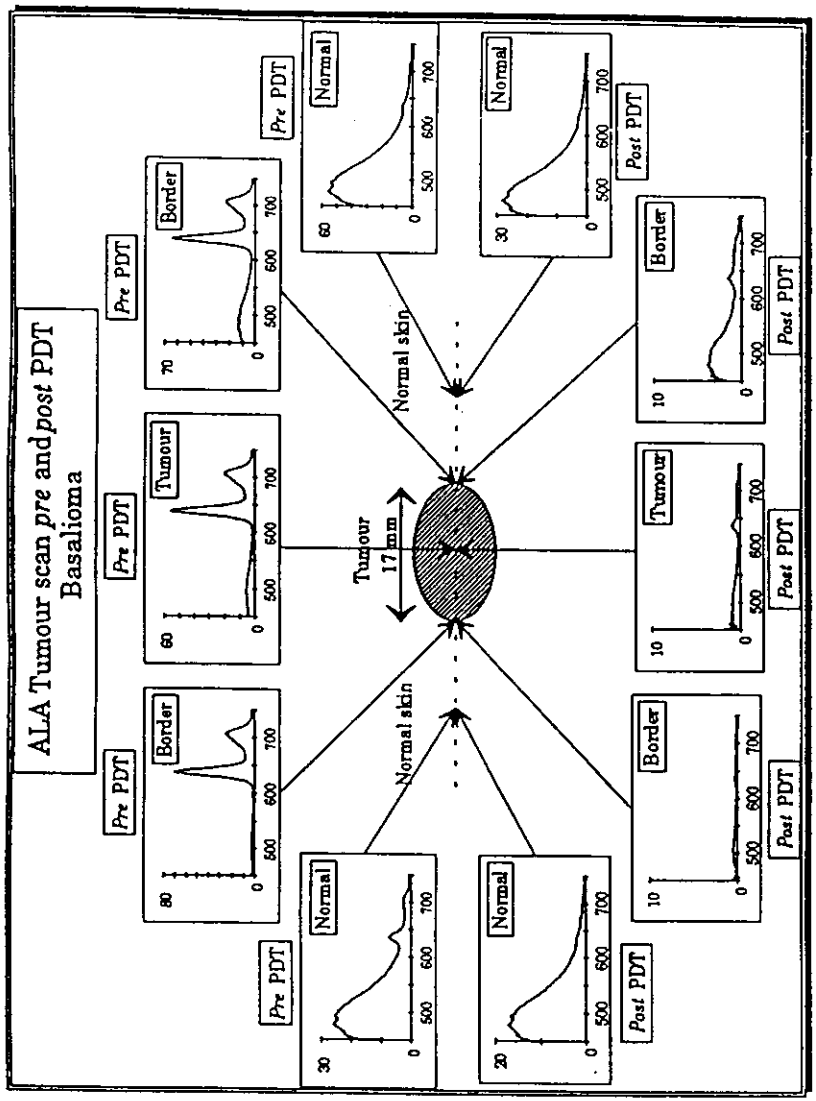

Figure 15.

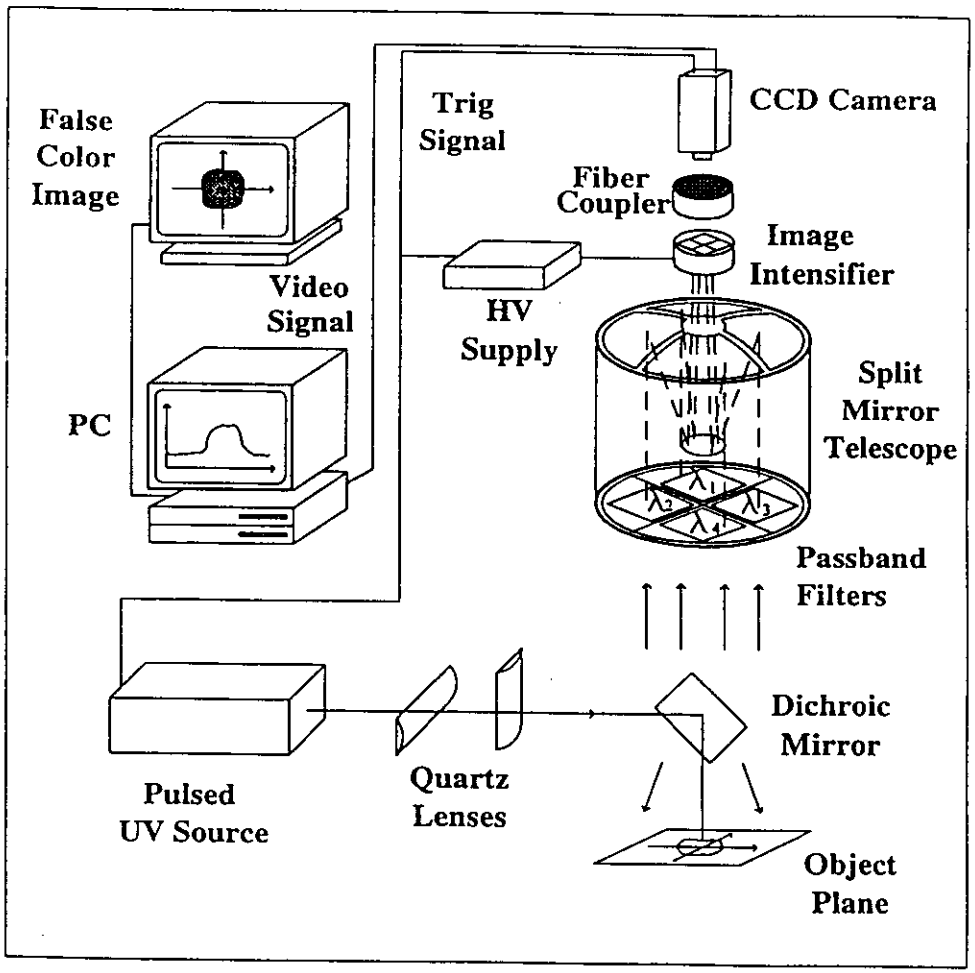

Figure 16.

ath in Western countries.
ich as hypertension and
sis starts in the artery, the
n cell lining is thickened,
al stage, a fibrotic plaque
er in the process of the
the final stage calcium is
into a rigid, unflexible,
the plaque turns into a
erous blood cloths. An
21[61]. The peripheral as
ic disease. The change in
he basis for fluorescence

ssive procedures, such as
new modalities are now
ive procedures. A new
based catheters through a
for intra vasal treatment.
). The field is treated in
s have been used. Non-
ient of coronary arteries,
with UV ablation. Laser

as some problems which
ration and dissection are
follows all procedures
n over-reaction from the
ical as possible. Because
stem for the laser firing
inhibiting the laser power
a crude diagnostic signal
in Fig. 22. A calcified
nen the calcification has

8], that the fluorescence
narcating atherosclerotic
chromophore content in

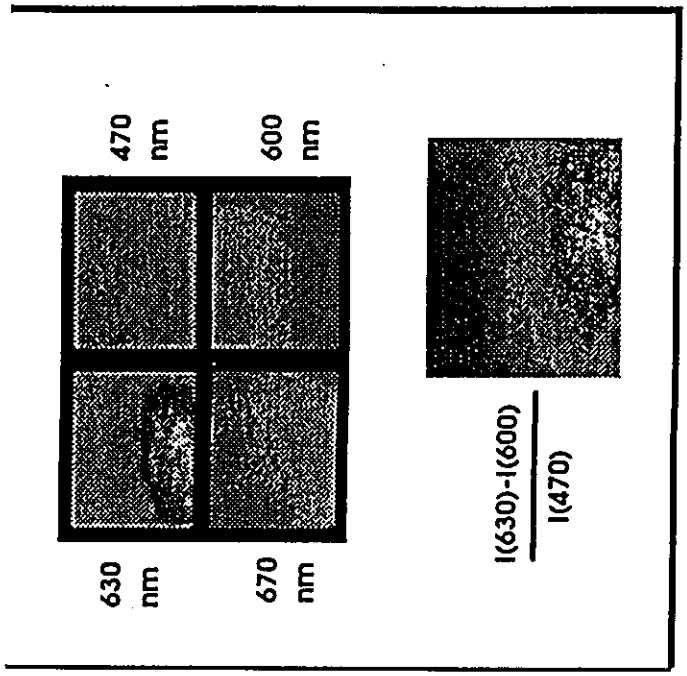

Figure 18.

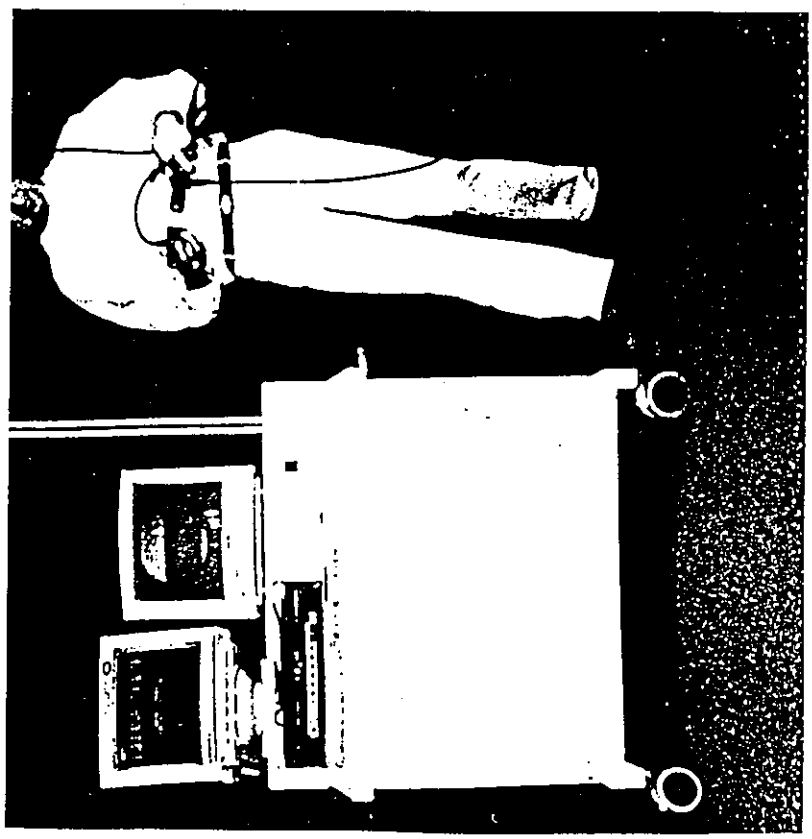

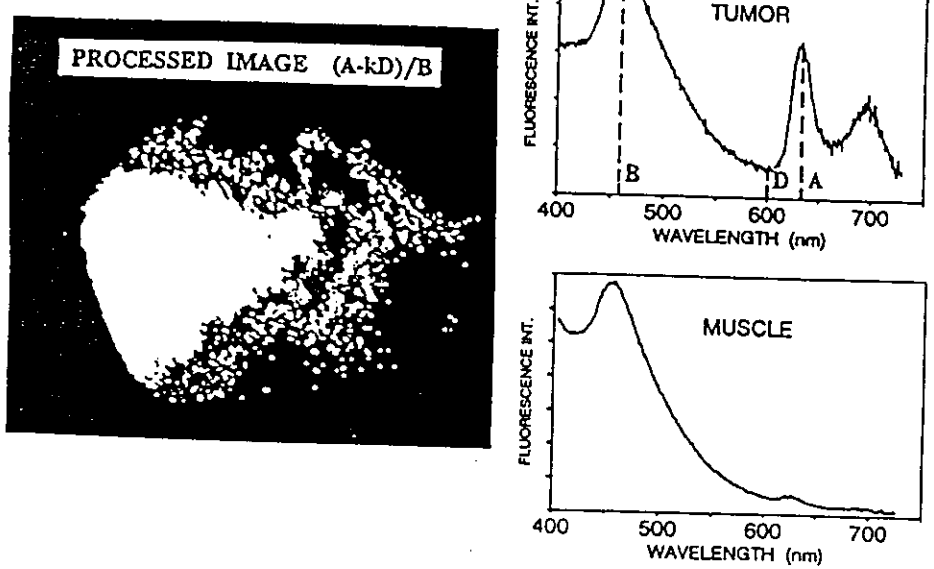
PROCESSED IMAGE (A-kD)/B
TUMOR
FLUORESCENCE INT.
B
D
A
400
500
600
700
WAVELENGTH (nm)
MUSCLE
FLUORESCENCE INT.
400
500
600
700
WAVELENGTH (nm)

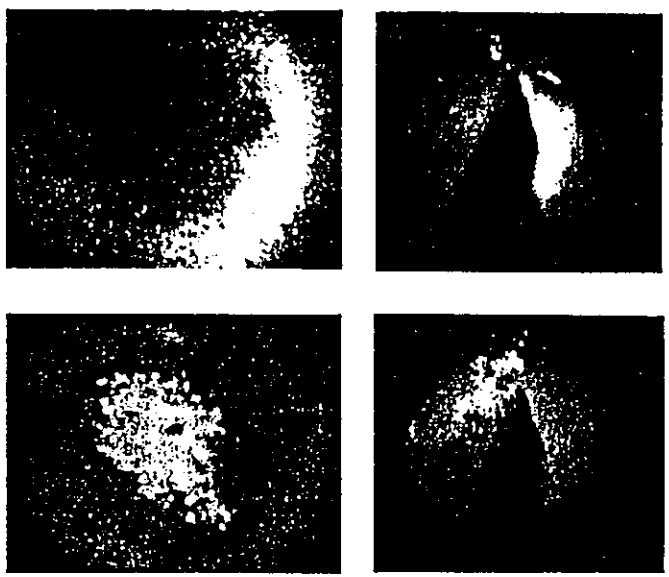

Figure 19

4. SPECTROSCOPIC DIAGNOSTICS OF ATHEROSCLEROTIC PLAQUE

4.1 Basic Considerations

Cardiovascular disease is, besides cancer, the major cause of death in Western countries. Several risk factors in the development of atherosclerosis, such as hypertension and smoking, have been identified. When the process of atherosclerosis starts in the artery, the innermost part of the vessel wall, the intima with the endothelium cell lining is thickened, and new constituents are deposited in the tissue. During the initial stage, a fibrotic plaque develops with increasing amount of collagen and elastin. Later in the process of the disease, cholesterol crystals and lipid droplets are deposited. In the final stage calcium is incorporated and the former elastic vessel tube is transformed into a rigid, unflexible, partly obstructed and brittle vessel. Sometimes the surface of the plaque turns into a wound, which easily can be an area for growth of dangerous blood cloths. An atherosclerotically affected vessel is schematically shown in Fig. 21[61]. The peripheral as well as the coronary arteries can be affected by the atherosclerotic disease. The change in chemical composition in the atherosclerotic vessel wall forms the basis for fluorescence diagnostics of this disease.

The surgical treatment of severe atherosclerosis includes aggressive procedures, such as open-heart surgery with coronary by-pass operation. Several new modalities are now being investigated as possible replacements for such extensive procedures. A new modality is laser based transluminal angioplasty, in which fiber based catheters through a peripheral artery, e.g. the femoral artery, are used as an entrance for intra vasal treatment. A schematic diagram of such a procedure is shown in Fig. 22[62]. The field is treated in detail in Chapter 11[6] of this volume. Different kinds of lasers have been used. Non-thermal excimer laser ablation is of special interest for the treatment of coronary arteries, as the thermal lasers induce artery spasm that might be avoided with UV ablation. Laser angioplasty is discussed in Refs 63-66.

Although promising, the laser based percutaneous angioplasty has some problems which must be overcome. In addition to arterial spasm, vessel wall perforation and dissection are complications that must be avoided. Another problem which follows all procedures performed in the vessel wall is re-stenosis, which is due to an over-reaction from the treated tissue. This might be minimised if the treatment is as radical as possible. Because the procedure is performed inside the vessel walls, a guiding system for the laser firing would improve the possibility of monitoring the procedure and inhibiting the laser power when the ablation has to be interrupted to avoid complications. A crude diagnostic signal is provided from the plasma emission signal as shown included in Fig. 22. A calcified plaque features strong lines of Ca and Ca^+ which disappear when the calcification has been ablated away[67,68].

4.2 Plaque Discrimination using Laser-Induced Fluorescence

It has been shown by several groups[69-73] and ourselves[74,68,28], that the fluorescence from the tissue itself, the autofluorescence, can be used in demarcating atherosclerotic lesions from non-diseased vessel wall, depending on the various chromophore content in

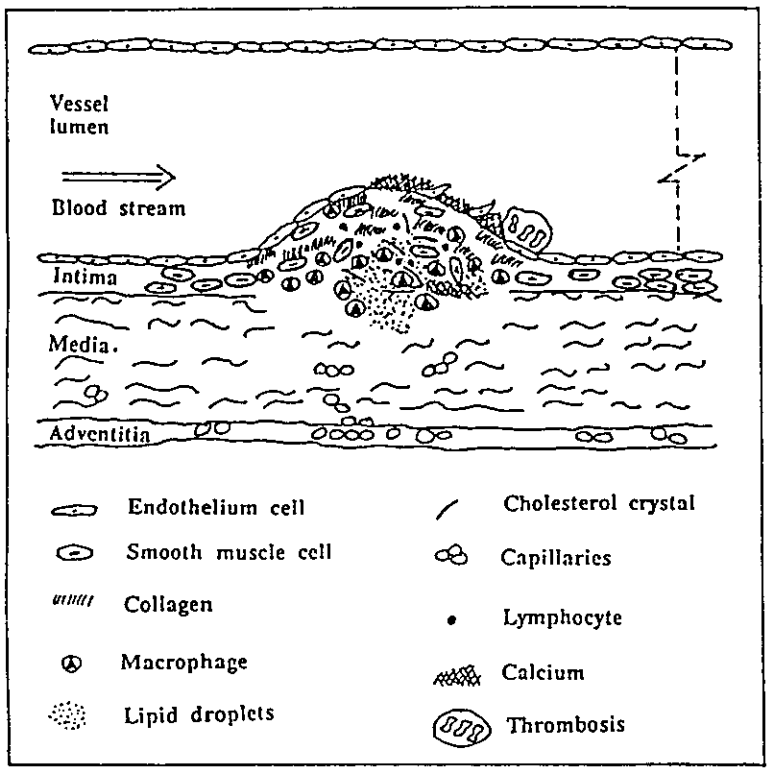

Figure 21.

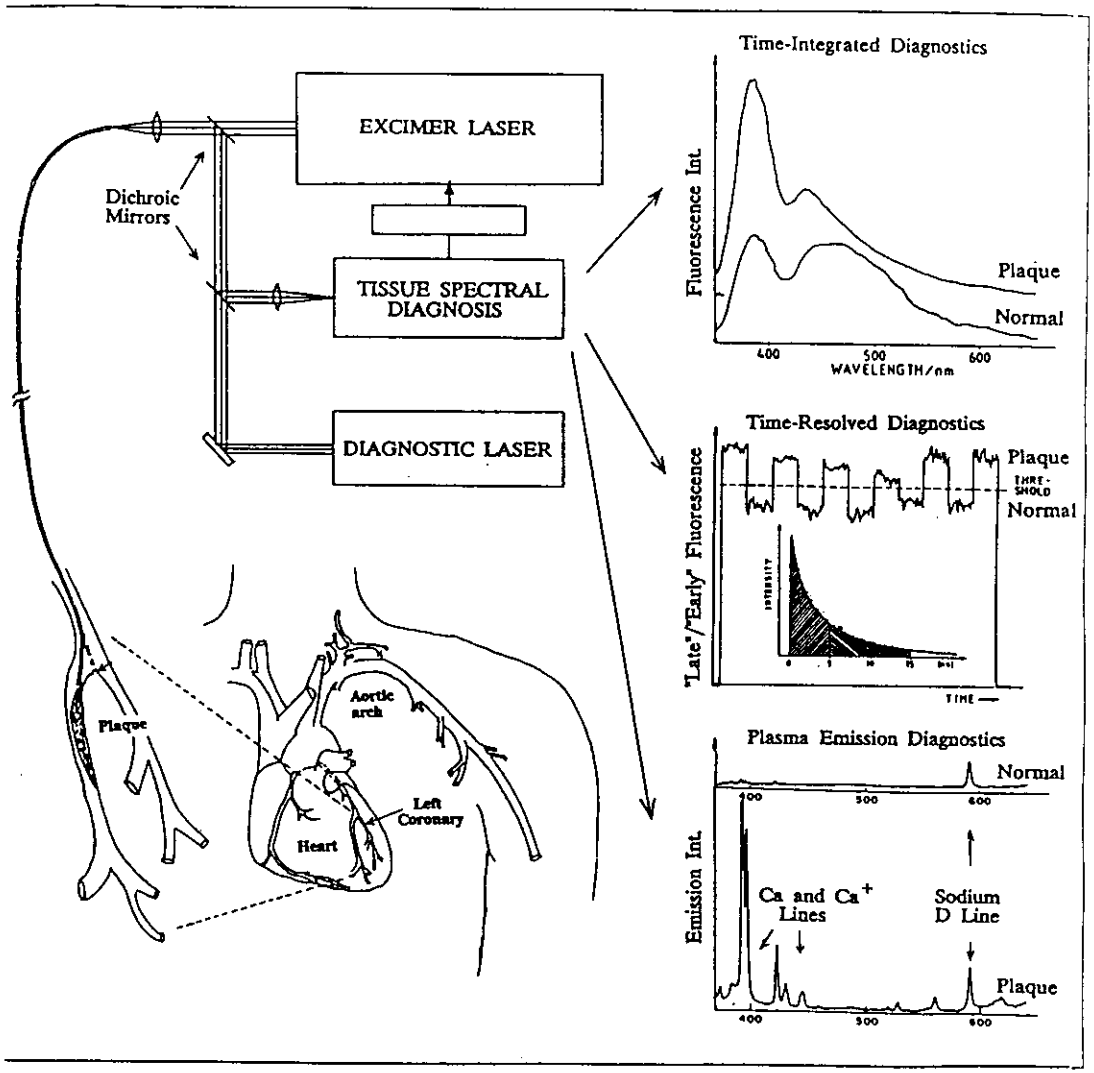

Figure 22.

the tissue types. The spectral shape of the tissue fluorescence can be used in demarcating the lesions, as the shape reflects the different molecular contents. Fluorescence provides a completely non-intrusive way of probing prior to firing a high-power pulse. When excited with the light from a UV laser, the normal vessel wall emits strong fluorescence in the region 390-500 nm, while atherosclerotic plaque has a prominent peak at 390 nm with a fall-off towards longer wavelengths. This is illustrated by the spectra included in Fig. 22. The signals are mainly built up from contributions of elastin and collagen (see Fig. 4a), with a relative increase in collagen in atherosclerotic plaque being the origin of the spectral difference. In both spectra, a minimum in the fluorescence signal can be seen at 420 nm, representing the strong absorption of haemoglobin in blood. Weaker absorption peaks occur at 540 and 580 nm. The identification of these features becomes very clear in a comparison with blood absorption spectra as shown in Fig. 23[28]. Clearly, the influence of the blood reabsorption must be handled properly by a reliable fluorescence diagnostic system.

We have in our investigations observed that the signature *in vitro* from a plaque region differs depending on the stage of the atherosclerotic process. The early fibrotic lesions can be separated from the plaque regions with higher fat content and also from calcified regions. We have been able to spectroscopically separate four different classes of atherosclerotic lesions depending on the severity of the disease. This is illustrated in Fig. 24[28]. The intensity ratios at selected wavelengths have been formed for a large number of samples. Group O is the normal non-diseased vessel wall tissue. Group I includes the least damaged tissue with only small amounts of fibrotic constituents. In group II more fibrotic constituents are present. Group III includes lesions with calcium content in the plaque, while in group IV calcium occurs at the surface. In this group (IV) the lesions with endothelial damage with or without thrombotic material on the damaged surface are included. In the figure all functions except F3 show a substantial demarcation between the tissue types. Functions F5 and F6 are particularly interesting, since they are immune to the presence of blood. This is because the wavelength pairs chosen corresponds to points of equal blood absorption, as indicated in Fig. 23. Thus, in the ratio the influence of the absorption is largely eliminated[68,75,28].

Similar techniques can be used for studying myocardial tissue for assessing the status of the heart muscle. From a large number of biopsy samples it was found that normal myocardial tissue can be distinguished from scar or fatty tissue as shown in Fig. 25, where two fluorescence intensity ratios have been used for the demarcation[76].

Some *in vivo* investigations were performed in connection with coronary by-pass procedures using a clinically adapted fluorosensor system as shown in Fig. 26. The system displays the ratio of the signal intensities for the blood-independent wavelength pair 380 and 440 nm. The fiber probe of the system was placed at the location where the coronary arteries were opened in order to be attached to the new vessels. Investigations were also performed inside the coronary arteries in the peripheral direction with the probe inserted into the lumen towards known occlusions. Fluorescence was also measured from normal aortic wall close to the heart. A recording using this system is shown in Fig. 27[77].

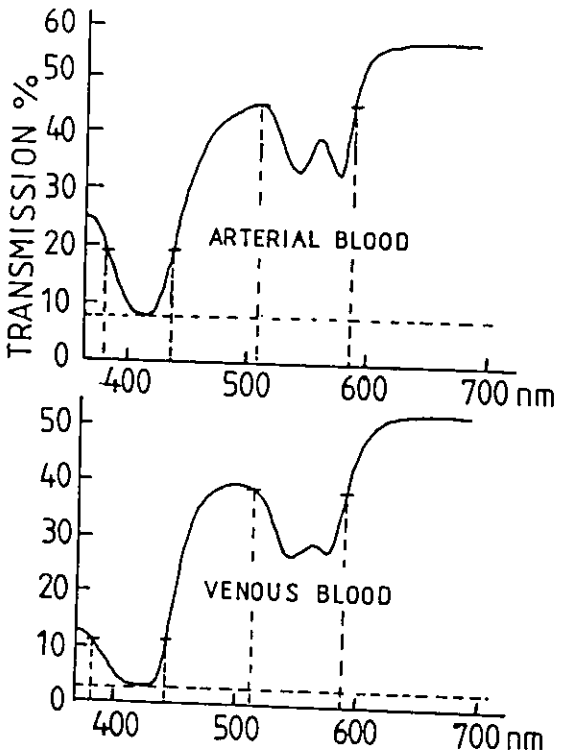

Figure 23.

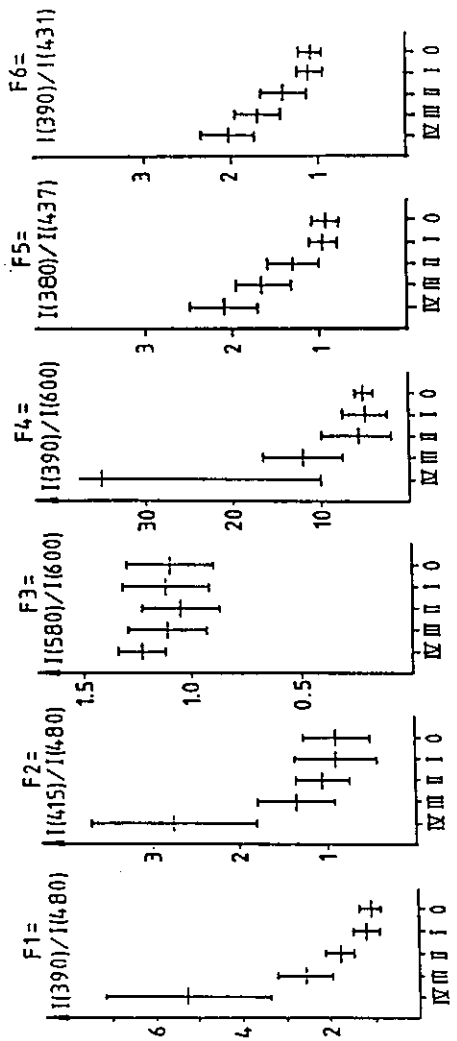

Figure 24.

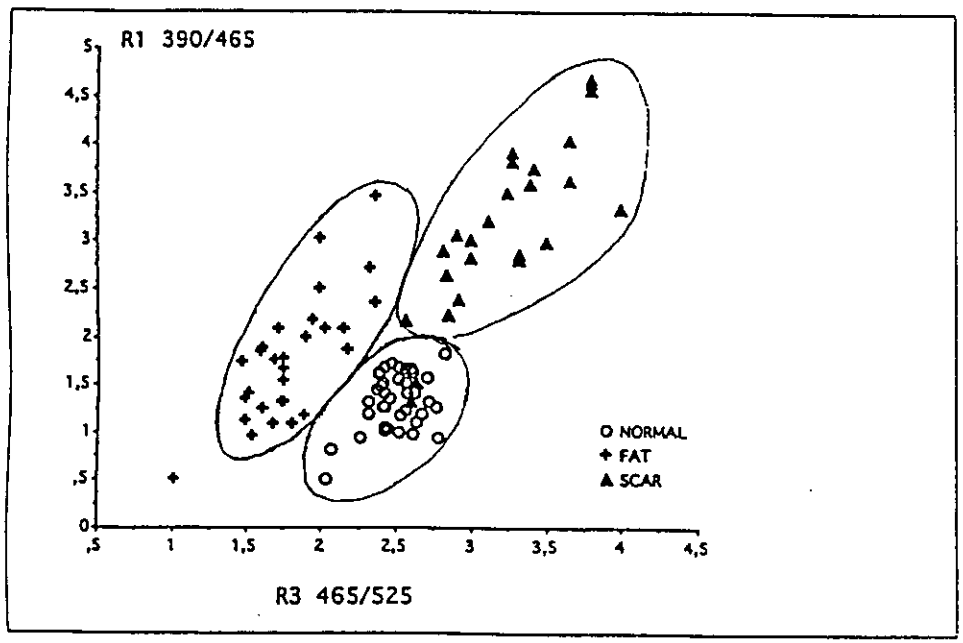

Figure 25.

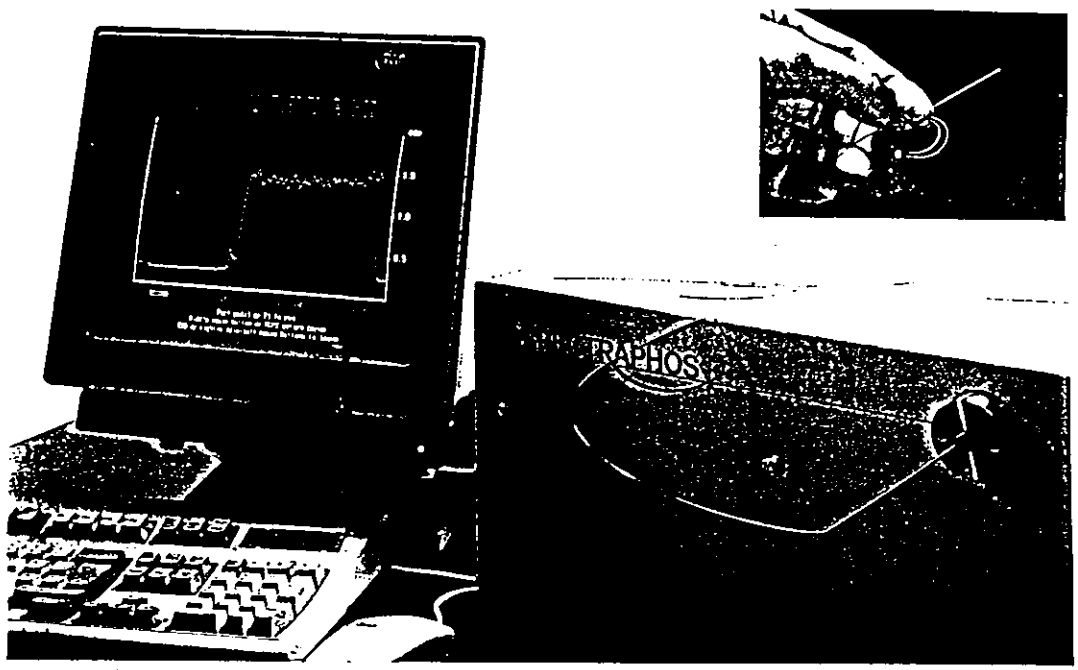

Figure 26.

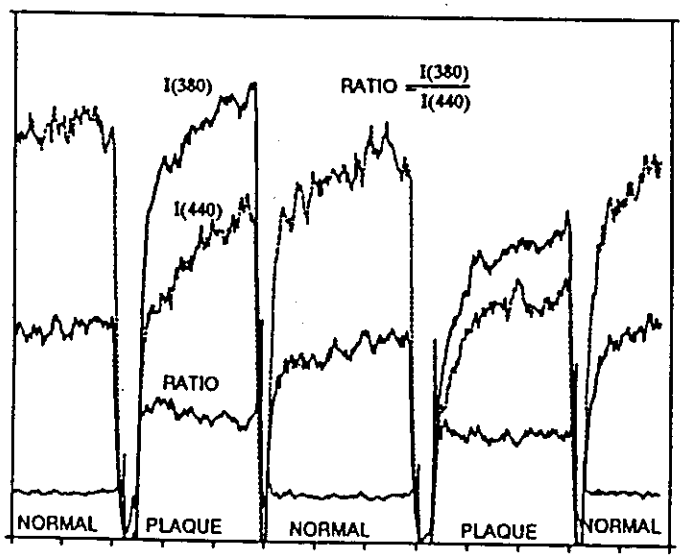

Figure 27.

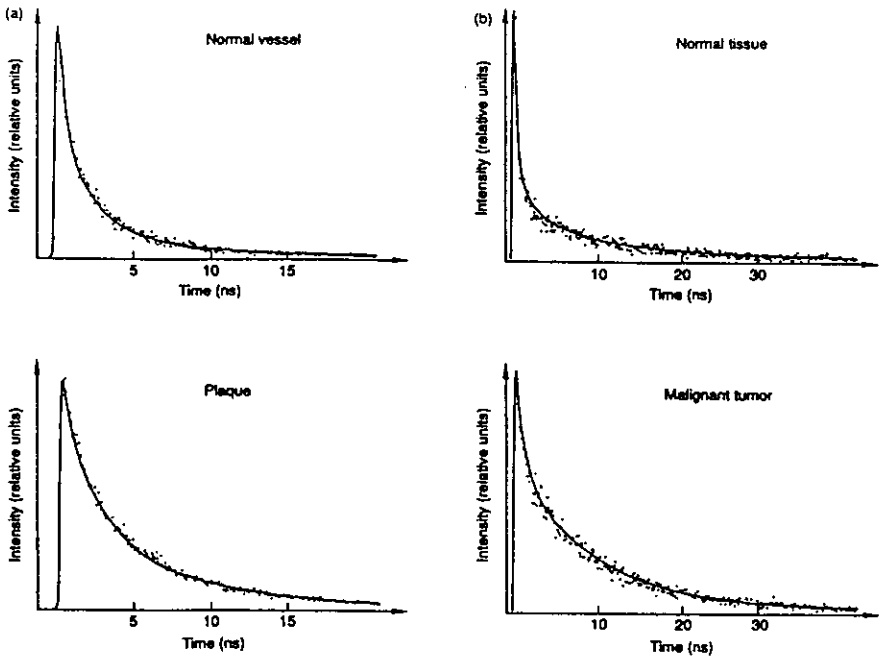

Figure 28.

4.3 Time-Resolved Monitoring

In all the fluorescence measurements discussed so far the total fluorescence intensity following pulsed laser excitation has been used. However, the temporal decay characteristics of the fluorescence light may also be utilised for tissue characterisation, e.g. for distinguishing atherosclerotically diseased vessel wall from normal vessel wall[75,78,28,13]. The fluorescence from the diseased region has a longer decay time compared to the normal vessel wall tissue as shown in Fig. 28. The reason for this is basically that collagen, more abundant in plaque, has a longer lifetime than elastin. These recordings were taken with an advanced set-up incorporating a mode-locked picosecond laser source in conjunction with time correlating photon-counting electronics. By a detailed analysis it is possible to unfold the decay into three components with different decay times[78]. However, since the lifetimes involved are of the order of ns it is for a clinically practical device also possible to use a normal nitrogen laser with a pulse duration of about 3 ns and use gated integrators to capture "late" fluorescence (5-15 ns) and divide it by "early" fluorescence (0-5 ns). A recording obtained in this way when moving the fibre tip alternatingly between plaque and normal wall is included in Fig. 22. Since a single detection wavelength is used and since blood is non-fluorescing the data obtained are immune to the presence of blood, if the blood layer is not so thick that the whole signal is blocked out. A system based on the spectroscopic characterisation of diseased tissue for guiding purposes in percutaneous laser angioplasty could of course include time-integrated as well as time-resolved aspects in order to improve the classification ability. As a matter of fact, an instrumentation of the type shown in Fig. 26 allows both these aspects to be utilised.

Decay curves detected at 630 nm for an experimental tumor and surrounding normal issue are also included in Fig. 28. The animal had earlier been injected by Photofrin. It can be seen that the tumor curve has a fast and a slow decay component, while normal tissue only has a fast decay. The fast component corresponds to the tissue autofluorescence whereas the more long-lived component is due to the HPD drug. As was noted in Ref. 28, gating on late fluorescence yields suppression of the autofluorescence and contrast enhancement using a single detection wavelength.

4.4. Raman Spectroscopy for Tissue Diagnostics

Raman spectroscopy has long been a powerful tool used by chemists in the analysis of complex organic molecules. The techniques of Raman spectroscopy are now being adopted for tissue spectroscopy[79-81]. As mentioned above, the main difficulty with this technique is the weakness of the signals and the competing process of fluorescence, which normally tends to completely swamp the Raman signals. An efficient way to reduce the influence of fluorescence is to use a laser with a near-IR wavelength, which does not excite fluorescence very efficiently. A CW Nd:YAG laser (λ=1064 nm) in combination with a Fourier transform spectrometer provides an efficient way of recording Raman spectra[82]. A clinically more practical way is to use a near-IR diode laser in combination with a cooled near-IR CCD array[80]. A different way to suppress fluorescence is to use a picosecond laser source and limit the detection to the duration of these short pulses. Then fluorescence, which typically has a lifetime of few ns, is reduced while all the Raman photons are recorded, since the latter process is basically instantaneous. This procedure can, however, hardly replace the use of a near-IR laser.

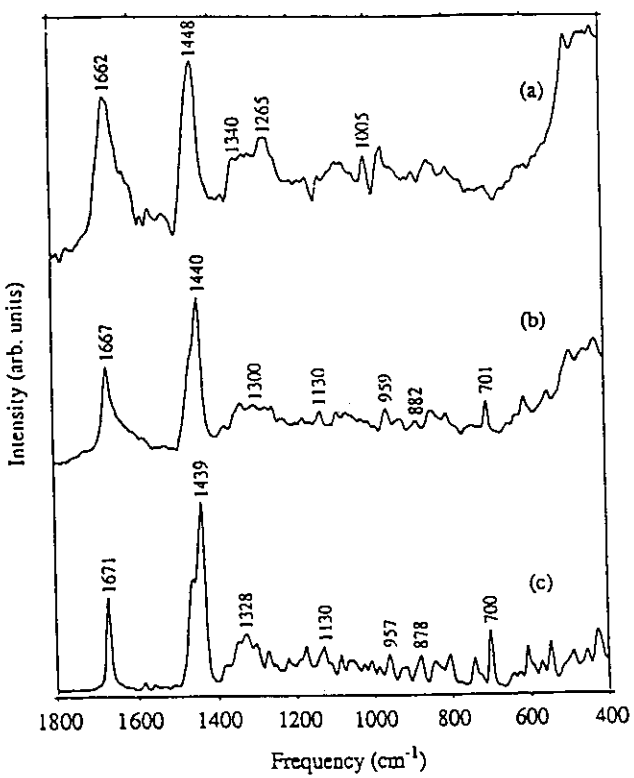
Intensity (arb. units)
1662
1448
1340
1265
1005
(a)
1667
1440
1300
1130
959
882
701
(b)
1671
1439
1328
1130
957
878
700
(c)
1800
1600
1400
1200
1000
800
600
400
Frequency (cm-1)

Figure 29

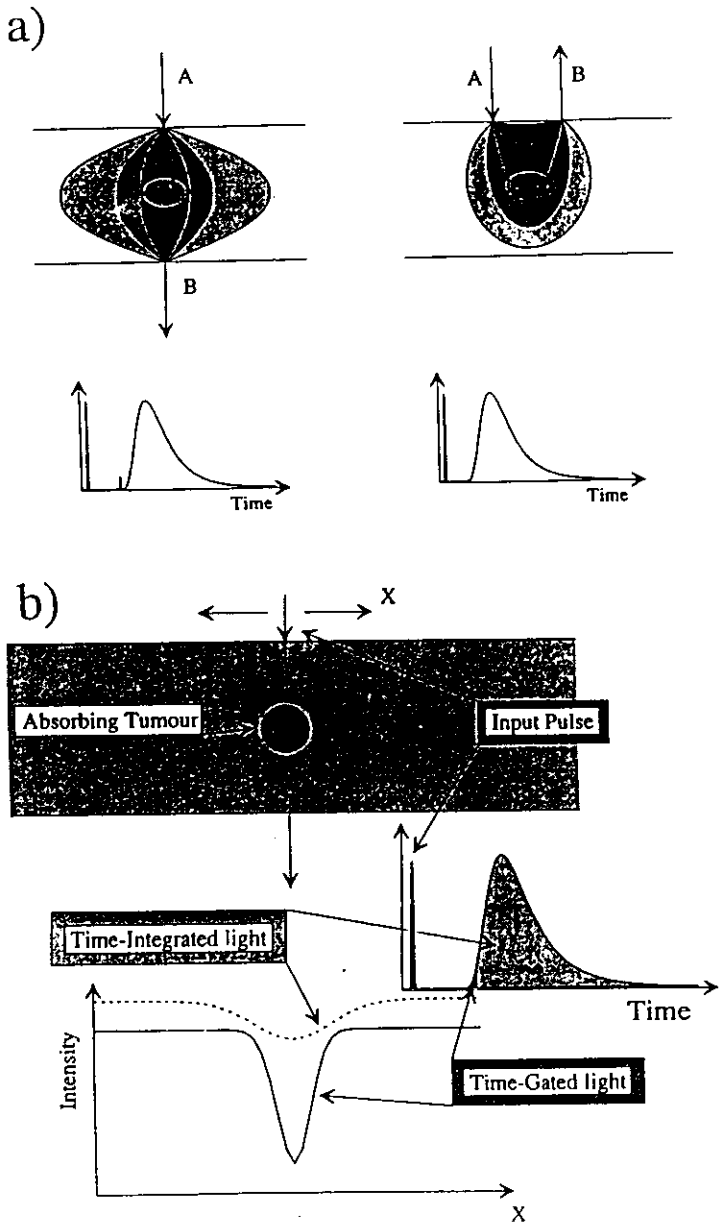
a)
A
B
Time
A
B
Time
b)
X
Absorbing Tumour
Input Pulse
Time-Integrated light
Time
Intensity
Time-Gated light
X

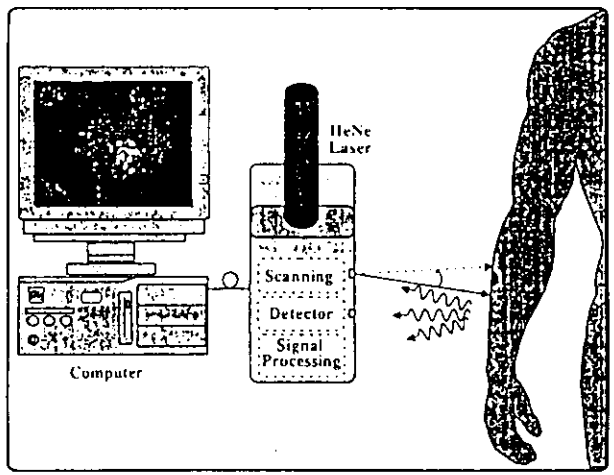

The arrangement of the laser Doppler perfusion imaging (LDPI) system.

Figure 31.

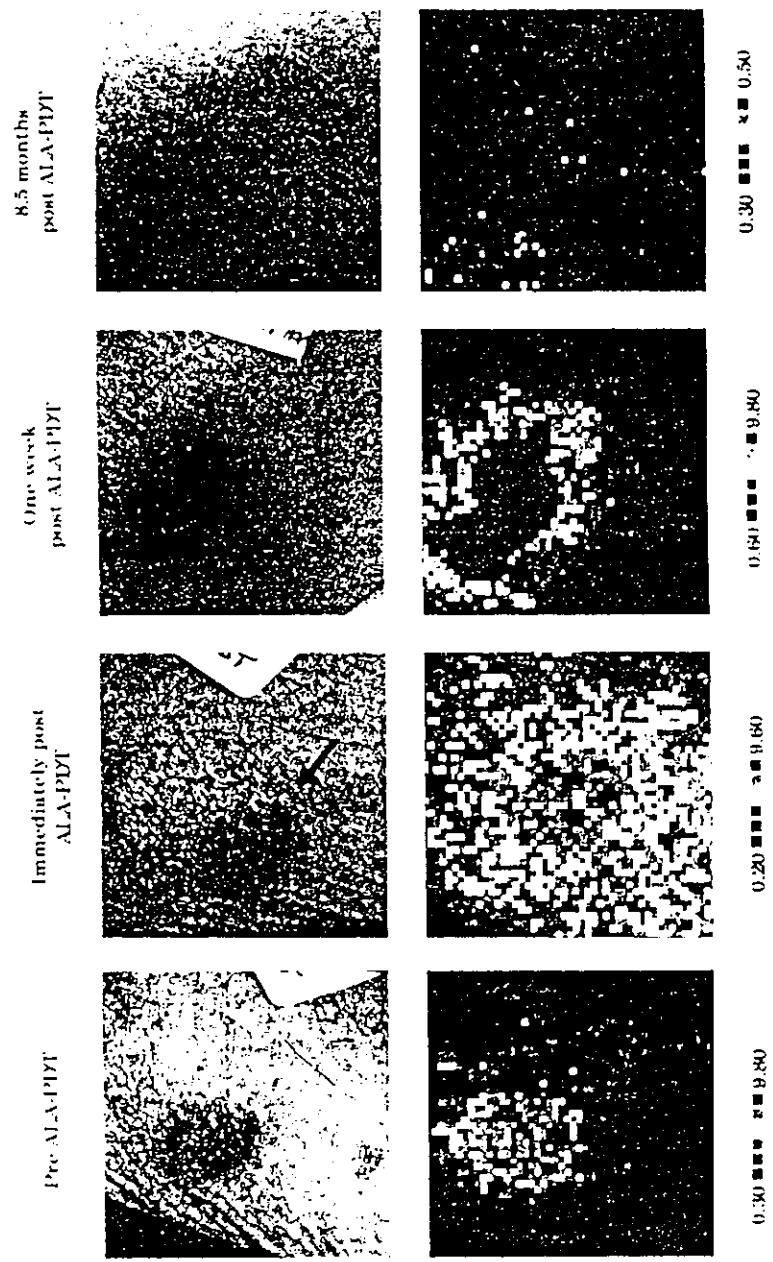

Figure 32.

depth. Still, using experience, valuable information can be obtained, in particular for assessing reperfusion in connection with transplant surgery. The techniques and clinical application of laser Doppler blood flowmetry can be found in Refs 20,21.

By performing sequential measurements with a system, where the laser beam is scanned in a matrix pattern over the tissue it is possible to generate images of the superficial blood flow[86]. A schematic diagram of such a system is shown in Fig. 31[86]. An example of the application of such a system is shown in Fig. 32[87], where the blood flow in a tumor region is shown in connection with PDT. Matching normal photos are also shown. A squamous cell carcinoma *in situ* (Bowen´s disease) was treated after topical application of ALA. The perfusion image is shown on four occasions. First an image before the treatment was taken, exhibiting an increased blood flow localized to the tumor region. Directly after PDT (60 J/cm^2), given at such a low laser light fluence rate so that tissue heating is avoided, an increased blood flow is seen in the tumor and surrounding area, indicating an immediate inflammatory tissue response. One week after the treatment a renewed imaging of the area shows a high blood flow restricted to the tumor and its close surrounding. Finally, 8.5 months after PDT the tumor in visibly absent and the blood flow is strongly reduced.

5.2 Time-Resolved Scattering Spectroscopy

As mentioned above, time-resolved transillumination allows enhanced viewing through tissue. X-ray diagnostic techniques are the conventional means for such imaging that has been brought to a very high level of sophistication. However, ionizing radiation is accompanied with a certain risk of mutagenicity [88]. It would be very desirable to use optical radiation for transillumination of tissue to avoid this risk and also to allow spectroscopic recordings of molecular-specific absorption. Red light penetrates tissue quite well as can be evidenced when shining light from a flash light through a hand of a child. The reason is the quickly decreasing absorption of haemoglobin beyond 600 nm as is illustrated by the corresponding curve in Fig. 1. The low intensity of the transmitted light through thick tissue is not a problem, since very sensitive light detectors exist, but rather the strong multiple scattering from the cell structures, washing out all the spatial information. Scattering prevents the observation of the bones in the hand as shadows. The scattering has limited the application of optical transillumination (diaphanography) for mammographic investigations[89-91]. Only superficial tumors close to the skin in the breast parenchyma can be made visible. Recently, a lot of research has been initiated to overcome these problems [92,85], e.g. by using time-resolved photon-counting techniques employing picosecond red laser pulses[93-96]. Because of the multiple scattering, most of the photons penetrating the tissue have spent a long time in the tissue, while only very few photons arrive to the detector at the nominal propagation time without disruptions. However, by selecting a very small detection time window and recording the very first photons, it is possible to look at just the "fastest" photons coming out of the tissue. If an obstacle, such as a bone or a tumor blocks the passage, a shadow will be created for the selected subgroup of very early photons. For thicker samples there are no unscattered photons. Still, the first photons have been minimally scattered producing a more clear image, as schematically shown in Fig. 30b. An example of a scan through a human hand is shown in Fig. 33[94]. A cavity dumped dye laser, synchronously pumped by an argon-ion laser, was used in these measurements. Time-gated single-photon counting was used

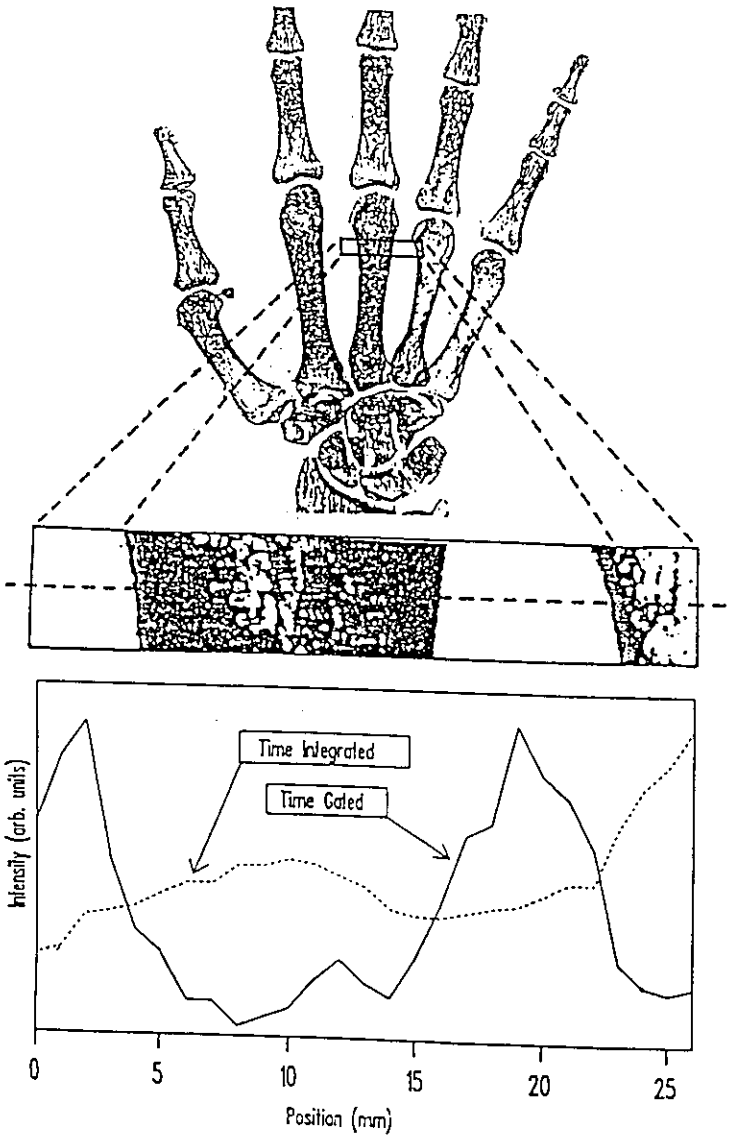

Figure 33

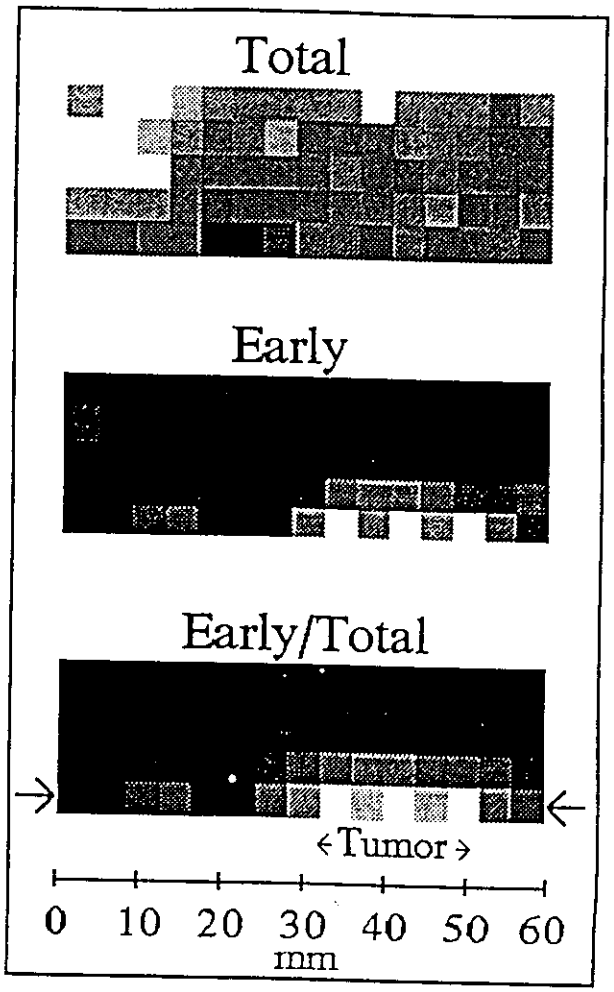

Figure 34

to record "early" photons in a time window 80 ps wide. Clear shadows of the bones can be seen in the time-gated scan, while the contrast disappears in the time-integrated recording.

5.3 Transillumination Imaging

By scanning the tissue under investigation, a transillumination image can be created. Recently we have shown, that such measurement can also be performed using a pulsed diode-laser source making the technique very realistic[96]. Images of a ductal breast carcinoma in a newly resected breast are given in Fig. 34. A diode laser, operating at 815 nm and producing 30 ps long pulses at a repetition rate of 10 MHz was used in these recordings, performed with the set-up shown in Fig. 35. The transmitting and receiving fibers are scanned together under computer control over the tissue, that is compressed between glass plates. In the time-integrated light the tumor cannot be seen. It was also difficult to detect using conventional X-ray mammography. In the time-gated image the tumor can be clearly seen. In order to eliminate possible artefacts it is advantageous to divide the early light by the total light as also shown in the figure.

Many groups are now working in this new field of research developing a variety of techniques for suppressing excessive scattering using streak-camera[97], Raman-amplifier[98] and frequency-doubling gating[99]. Fast modulation of the source followed by detection of phase-shifts and loss of modulation depth can give similar information[100-102]. The coherence properties of non-scattered light are used in heterodyne[103] and light-in-flight holography[104,105]. Imaging in scattering media can also be performed with spatial domain reflectometry[106,107].

5.4. Interpretation of Time-Resolved Tissue Recordings

In this section we will focus on the interpretation of time-resolved recordings of tissue in order to understand. e.g. how tumors can be detected in the early light. This is best performed by examining the results of a model experiment[95], performed with picosecond pulses traversing a 30 mm thick cuvette, containing a mixture of Intralipid (Kabi Vitrum) and ink in water. Intralipid is a strongly scattering, non-absorbing liquid, while ink has a strong absorption but negligible scattering. By mixing these two substances the values of the scattering and absorption coefficients, μ_s and μ_a, can be varied freely. In the upper part of Fig. 36, time-resolved recordings can be seen, where no ink but increasing amounts of Intralipid have been added. It can be seen, that at early times the time dispersion curves are strongly influenced, while the "decay constant" at late times is little affected. If, on the other hand, increasing amounts of ink is added for a constant amount of Intralipid, it can be seen, in the lower part of Fig. 36, that the early light is basically unaffected, while the "decay constant" for the late light is quickly shortened for increasing absorption. In the figure an early, fixed detection window is indicated. Using these curves the increasing signal for tumor in Fig. 34 (brighter areas) can be interpreted as a reduction in the scattering in a tumor rather than a change in the absorption. This means, that the early light is not useful for absorption spectroscopy changing the wavelength. On the other hand, wavelength dependent scattering changes might prove useful for tissue identification. The decay constant for the late light is related in a simple way to the absorption coefficient[108]. However, for this "late" light little

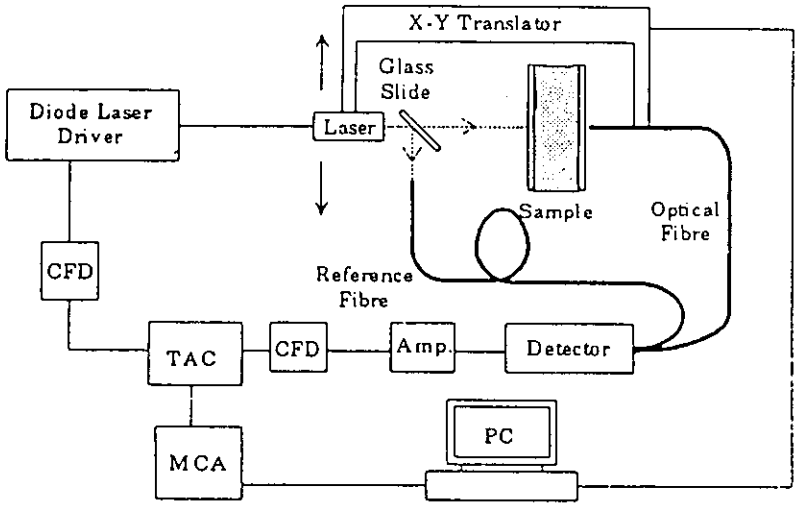

Fig. 35 *Experimental set-up for gated viewing using delayed-coincidence techniques. CFD: constant fraction discriminator. TAC: time-to-amplitude converter. MCA: multichannel analyzer. Amp.: amplifier. PC: computer.*

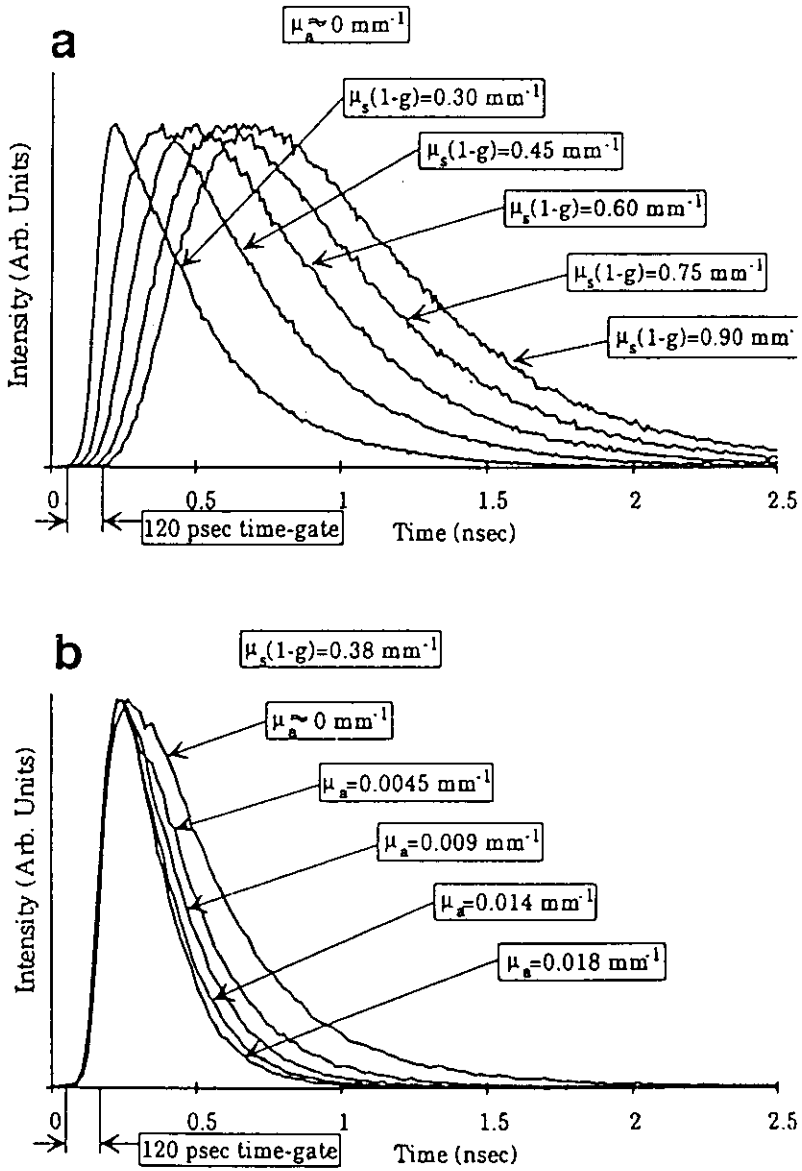

Fig. 36

image information is retained. By using the whole temporal dispersion curve, maximal tissue information can be extracted, using wavelength dependent properties of different chromophores and tissue structures.

Focusing on the properties on the late light, spectroscopic analysis has been performed[15] for assessing the concentration of photosensitizers in tumors for PDT light dosimetry. Then light with a wavelength on the sensitizer absorption peak as well as light off that peak is analysed. The first time-resolved measurements on human tissue concerned brain oxygenation assessment, e.g. in premature infants, by using differences in oxy- and deoxyhaemoglobin absorption[108-110] (See Figs 1 and 23).

At the end of this section we should note, that tissue information can be obtained also when time-integrating instrumentation is used, e.g. when a CW light source is employed. As we have noted, the path length is not well defined due to multiple scattering in the tissue. Still, equipment used in a standardised way can yield reliable data. An example of this is the blood oxygenation measurements performed with a pulse oximeter, where light is sent through a finger tip of the patient, probing the differential absorption of oxy- and deoxyhemoglobin[111]. Normally, light at three different wavelengths are used, generated by light-emitting diodes or diode lasers. 805 nm provides a reference point, where oxy- and deoxyhemoglobin absorb equally much (the isobestic point). At 660 and 940 nm the two types of haemoglobin have very different absorptions. The oxygenation value (oxygen tension) obtained with a pulse oximeter has been shown to be influenced by the hematocrite value (density of red blood cells) and by complex formation in the blood of smokers. Even if the absolute value is subject to various influences, the instrument has an important application in monitoring of patient status from the time before anaesthesia through an operation, or during bronchoscopy. A further example of a CW method is a technique for cancer diagnostics where the elastically scattered light from a broad-band source is analysed at some distance from the point of light injection into the tissue[112]. Since the scattering properties vary for different types of tissue, the signal recorded can be compared with catalogue spectra obtained for well characterised tissues. Thus a tissue diagnosis can be obtained in this empirical way.

6. OUTLOOK

As illustrated in this chapter, many new possibilities of tissue diagnostics using lasers are emerging, addressing important fields such as cancer detection, cardiovascular monitoring and tissue transillumination imaging without using ionizing radiation. The rapid development of more and more practical and cost-effective laser sources, detectors and computers facilitates the clinical implementation of the new techniques. The non-invasive nature of the techniques and the real-time data acquisition are attractive features of the optical methods. Optical spectroscopy in principle allows molecular analysis, providing information not normally accessible with other modalities. For the future an increased use of combined diagnostic and therapeutic equipment can be anticipated. Ideally, each single cell should be optically diagnosed followed by an immediate decision if that cell should be eliminated using promptly following laser ablation, heating or photochemistry.

7. ACKNOWLEDGEMENTS

The author gratefully acknowledges a most stimulating collaboration with a large number of colleagues and graduate students within the Lund University Medical Laser Center, as well as with many foreign groups. This work was supported by the Swedish Research Council for Engineering Sciences, The Swedish Board for Technical and Industrial Development, the Swedish Cancer Foundation and the Swedish Medical Research Council.

REFERENCES

1. R. S. Mackay, Medical Images and Displays: Comparison of Nuclear Magnetic Resonance, Ultrasound, X-rays and other Modalities, Wiley, New York (1984).

2. S. Svanberg, Atomic and Molecular Spectroscopy, 2nd ed., Springer, Heidelberg (1992).

3. J.-L. Boulnois, Photophysical processes in laser-tissue interactions, in: Laser Applications in Cardiovascular Diseases, (R. Ginsberg, ed.), Futura, New York (1987).

4. H.C. Chen, Space Remote Sensing Systems, Academic, Orlando (1985).

5. K. Thompson, Lasers in ophthalmology, in: Lasers in Medicine, (G. Pettit and R.W. Waynant, eds), Wiley, New York (1995).

6. J. Haller, Lasers in cardiology, in Lasers in Medicine, (G. Pettit and R.W. Waynant, eds), Wiley, New York (1995).

7. S. Svanberg, Medical applications of laser spectroscopy, Physica Scripta T26, 90-98 (1989).

8. S.L. Marcus, in Photodynamic Therapy of Human Cancer: Clinical Status, Potential and Needs, (C. Gomer, ed.), pp. 1, SPIE Press, Bellingham (1990).

9. H.I. Pass, Photodynamic therapy in oncology: mechanisms and clinical use, J. National Cancer Inst. 85, 443-456 (1993)

10. S.L. Marcus, Lasers in photodynamic therapy, in: Lasers in Medicine, (G. Pettit and R.W. Waynant, eds), Wiley, New York (1995).

11. J.R. Lakowicz, Principles of Fluorescence Spectroscopy, Plenum, New York, (1983).

12. O.S. Wolfbeis (ed.), Fluorescence Spectroscopy: New Methods and Applications, Springer, Heidelberg (1992).

13. S. Andersson-Engels, A. Gustafson, J. Johansson, U. Stenram, K. Svanberg and S. Svanberg, An investigation of possible fluorophores in human atherosclerotic plaque, Lasers in Life Science 5, 1-11 (1992).

14. S. Andersson-Engels, J. Johansson, K. Svanberg and S. Svanberg, Fluorescence imaging and point measurements of tissue: applications to the demarcation of malignant tumors and atherosclerotic lesions from normal tissue, Photochem. Photobiol. 53, 897-814 (1991).

15. B.C. Wilson, M. S. Patterson, S. T. Flock and D. R. Wyman, Tissue optical properties in relation to light propagation models and in vivo dosimetry, in Photon Migration in Tissue, (B. Chance, ed.), pp. 24-42, Plenum, New York (1989).

16. M.S. Patterson, B. C. Wilson, and D. R. Wyman, The propagation of optical radiation in tissue. I. Models of radiation transport and their application, Lasers Med .Sci. 6, 155-168 (1991).

17. B.C. Wilson and G. Adam, A Monte Carlo model for the absorption and flux distributions of light in tissue, Med. Phys. 10, 824-830 (1983).

18. S. L. Jacques, Time resolved propagation of ultrashort laser pulses within turbid tissue, Appl. Opt. 28, 2223-2229 (1989).

19. S. Patterson, B. Chance and B.C. Wilson, Time resolved reflectance and transmittance for the non-invasive measurement of optical properties, Appl. Opt. 28, 2331-2336 (1989).

20. P. Å. Öberg, Laser-Doppler flowmetry, Critical Reviews in Biomedical Engineering 18, 125-163 (1990).

21. A.P. Shepherd and P.Å. Öberg (eds), Laser Doppler Blood Flowmetry, Kluwer Academic Publishers, Boston (1990).

22. Andersson-Engels, J. Ankerst, S. Montán, K. Svanberg and S. Svanberg, Aspects of tumour demarcation in rats by means of laser-induced fluorescence and haematoporphyrin derivatives, Lasers in Med. Sci., 3, 239-248 (1988).

23. S. Montán, On the use of laser-induced fluorescence in medical and industrial applications, PhD dissertation, Lund Reports on Atomic Physics LRAP-75, Lund University (1987).

24. G. Hedlund and H.O. Sjögren, Induction of transplantation immunity to rat colon carcinoma isografts by implantation of intact fetal colon tissue, Int. J. Cancer 26, 1-73 (1980).

25. J. Ankerst, S. Montán, K. Svanberg and S. Svanberg, Laser-induced fluorescence studies of hematoporphyrin derivative (HpD) in normal and tumor tissue of rat, Applied Spectroscopy 38, 890-896 (1984).

26. W. Lohmann, J. Mussmann, C. Lohmann and W. Kunzel, Native fluorescence of the cervix uteri as a marker for dysplasia and invasive carcinoma, Eur. J. Obstet. Gynecol. Reprod. Biol. 31, 249-253 (1989).

27. W. Lohmann and E. Paul, Native fluorescence of unstained cryo-sections of the skin with melanomas and naevi, Naturwissenshaften 76, 424-426 (1989).

28. S. Andersson-Engels, J. Johansson, U. Stenram, K. Svanberg and S. Svanberg, Malignant tumor and atherosclerotic plaque diagnosis using laser-induced fluorescence, IEEE J. Quant. Electron. 26, 2207-2217 (1990).

29. K. Svanberg, E. Kjellén, J. Ankerst, S. Montán, E. Sjöholm and S. Svanberg, Fluorescence studies of hematoporphyrin derivative in normal and malignant rat tissue, Cancer Research 46, 3803-3808 (1986).

30. S. Andersson-Engels, A. Brun, E. Kjellén, S. Montán, L.G. Salford, L.-G. Strömblad, K. Svanberg and S. Svanberg, Identification of brain tumours in rats using laser-induced fluorescence and haematoporphyrin derivatives, Lasers in Med. Sci. 4, 241-249 (1989).

31. S. Andersson-Engels, Å. Elner, J. Johansson, S.-E. Karlsson, L. G. Salford, L.-G. Strömblad, K. Svanberg and S. Svanberg, Clinical recordings of laser-induced fluorescence spectra for evaluation of tumour demarcation feasibility in selected clinical specialities, Lasers in Med. Sci. 6, 415-424 (1991).

32. P.S. Andersson, S. Montán, T. Persson, S. Svanberg and S. Tapper, Fluorescence endoscope instrumentation for improved tissue characterization, Med. Phys. 14, 633-636 (1987).

33. L. Baert, R. Berg, B. van Damme, M.A. D'Hallewin, J. Johansson, K. Svanberg and S. Svanberg, Detection of superficial bladder cancer utilizing laser-induced fluorescence and low-dose haematoporphyrin derivative, Urology 41, 322-330 (1993).

34. S. Andersson-Engels, J. Johansson, D. Killander, E. Kjellén, L.O. Svaasand, K. Svanberg and S. Svanberg, Photodynamic therapy and simultaneous near-infrared light-induced hyperthermia in human malignant tumors - a methodological case study, Proc. ICALEO'87, 60, 67-74 (1987).

35. S. Andersson-Engels, J. Johansson, D. Killander, E. Kjellén, M. Olivo, L.O. Svaasand, K. Svanberg and S. Svanberg, Photodynamic therapy alone or in conjunction with near-infrared light-induced hyperthermia in human malignant tumors: a methodological case study, Proc. SPIE 908, 116-125 (1988).

36. Andersson-Engels, R. Berg, S. Colleen, J. Johansson, S.E. Karlsson, R. Lundgren, L.G. Salford, L.-G. Strömblad, K. Svanberg, and S. Svanberg, *In vivo* fluorescence spectra of malignant lesions in various clinical specialities, In: Photodynamic Therapy and Medical Laser Applications, (P. Spinelli, ed.), Elsevier, Amsterdam (1992).

37. S. Andersson-Engels, E. Bak-Jensen, R. Berg, S. Colleen, R. Lundgren, K. Svanberg, S. Svanberg, Photofrin distribution in malignant tumours of the prostate, Progress Report 1992, Lund University Medical Laser Centre, p. 32, Lund University (1993).

38. S. Andersson-Engels, J. Johansson, S. Svanberg, S.-E. Karlsson, K. Svanberg and L. Johansson, Progress Report 1992, Lund University Medical Laser Centre, p. 30, Lund University (1993).

39. Ye Yanming, Yang Yuanlong, Xia Jinfang, Li Fuming and Li Yufen, Single pulse cancer diagnosis by laser excited autofluorescence, Chinese Physics - Lasers 14, 284 (1987).

40. Yang Yuanlong, Ye Yanming, Li Fuming, Li Yufen and Ma Baozhang, Characteristic autofluorescence for cancer diagnosis and its origin, Lasers Surg. Med. 7, 528-532 (1987).

41. R.R. Alfano, D.B. Tata, J. Cordero, P. Tomashefsky, F.W. Longo and M.A. Alfano, Laser induced fluorescence spectroscopy from native cancerous and normal tissue, IEEE J. Quant. Electr. QE-20, 1507-1511 (1984).

42. W. S. Glassman, C.H. Liu, G.C. Tang, S. Lubicz and R.R. Alfano, Ultraviolet exited fluorescence spectra from non-malignant and malignant tissues of the gynecological tract, Lasers Life Sci 5, 49-58 (1992).

43. R. Richards-Kortum, R.P. Rava, R.E. Petras, M. Fitzmaurice, M. Sivak and M.S. Feld, Spectroscopic diagnosis of colonic dysplasia, Photochem. Photobiol. 53, 777-786 (1991).

44. J. Hung, S. Lam, J.C. LeRiche and B. Palcic, Autofluorescence of normal and malignant bronchial tissue, Lasers Surg. Med. 11, 99-105 (1991).

45. R.R. Alfano, A. Pradhan, G.C. Tang, B.B. Das and K.M. Yoo, Optical spectroscopy may offer novel diagnostic approaches for the medical profession, in Laser Non-Surgical Medicine, I. Goldman (ed.), pp. 55-123, Technomic Publ., Lancaster (1991).

46. J.C. Kennedy, R.H. Potter and D.C. Pross, Photodynamic therapy with endogenous protoporphyrin IX: Basic principles and present clinical experience, J. Photochem Photobiol. 6, 143-148 (1990).

47. K. Svanberg, T. Andersson, D. Killander, U. Stenram, S. Andersson-Engels, R. Berg, J. Johansson, and S. Svanberg, Photodynamic therapy of non-melanoma cancers of the skin utilizing topical d-amino levulinic acid application and laser irradiation, Brit. J. of Dermatology 130, 743-51 (1994).

48. R. Berg, J. Johansson, D. Killander, K. Svanberg, S. Svanberg and Yang Yuanlong, Photodynamic therapy in interplay with fluorescence diagnostics in the treatment of human superficial malignancies, SPIE Vol.1645, 187 (1992).

49. K. Svanberg, T. Andersson, D. Killander, S. Andersson-Engels, R. Berg, J. Johansson, S. Svanberg and Yang Yuanlong, Photodynamic therapy of human skin malignancies and laser-induced fluorescence diagnostics utilizing Photofrin and δ-amino levulinic acid, in: Photodynamic Therapy and Medical Laser Applications, (P. Spinelli, ed.), Elsevier, Amsterdam (1992).

50. W.R. Potter, T.S. Mang and T.J. Dougherty, The theory of photodynamic therapy dosimetry: consequences of photodestruction of sensitizer, Photochem. Photobiol. 46, 97-101 (1987).

51. S. Montán, K. Svanberg and S. Svanberg, Multicolor imaging and contrast enhancement in cancer-tumor localization using laser induced fluorescence in hematoporphyrin-derivative-bearing tissue, Opt. Lett. 10, 56-58 (1985).

52. P.S. Andersson, S. Montán and S. Svanberg, Multispectral system for medical fluorescence imaging, IEEE J Quant. Electr. 23, 1798-1805 (1987).

53. S. Andersson-Engels, J. Johansson, and S. Svanberg, Multicolor fluorescence imaging system for fluorescence diagnostics, SPIE Vol. 1205, 179-189, Bellingham (1990).

54. S. Andersson-Engels, R. Berg, K. Svanberg and S. Svanberg, Multi-color fluorescence imaging in combination with photodynamic therapy of δ-amino levulinic acid (ALA) sensitized skin malignancies, to appear.

55. S. Andersson-Engels, R. Berg, J. Johansson and S. Svanberg, O. Jarlman, K. Svanberg and S. Montán, Fluorescence and transillumination imaging for tissue diagnostics, Proc. CLEO'91, Baltimore, April 1991, Opt. Soc. Am., Washington DC (1991).

56. K. Svanberg, I. Wang, S. Colleen, I. Idwall, Ch. Ingvar, R. Lundgren, R. Rydell, D. Jocham, A. Knipper, S. Thomas, H. Diddens, S. Bown, G. Gregory, S. Montán, I. Jonsson, S. Andersson-Engels and S. Svanberg, Clinical multi-colour fluorescence imaging of malignant tumours - Initial experience, to appear.

57. A.E. Profio, Review of fluorescence diagnosis using porphyrins, SPIE 907, 150-156, SPIE Optical Engineering, Bellingham, Wash. (1988).

58. G. Wagnières, Ch. Depeursinge, Ph. Monnier, M. Savary, P. Cornaz, A. Chatelain and H. van den Bergh, Photodetection of early cancer by laser-induced fluorescence of a tumor-selective due: apparatus design and realization, Proc. SPIE 1203, 43-52 (1990).

59. B. Palcic, S. Lam, J. Hung and C. Mac Aulay, Detection and localization of early lung cancer by imaging techniques, Chest 99, 742-43 (1991).

60. S. Lam, C. MacAulay, J. Hung, J. LeRiche, A.E. Profio and B. Palcic, Detection of dysplasia and carcinoma in situ with a lung imaging fluorescence endoscope device, J. Thorac. Cardiovasc. Surg. 105, 1035-40 (1993).

61. S. Andersson-Engels, R. Berg, J. Johansson, U. Stenram, K. Svanberg and S. Svanberg, Laser spectroscopy in medical diagnostics, in: Photodynamic Therapy: Basic Principles and Clinical Aspects, (Th. J. Dougherty and B.W. Henderson, eds), pp. 387-424, Marcel Dekker Inc., New York (1992).

62. K. Svanberg and S. Svanberg, Lasers in medicine, La RECHERCHE 255, 686-693 (1993).

63. J.M. Isner, P.G. Steg and R.H. Clarke, Current status of cardiovascular laser therapy, IEEE J Quant. Electr., QE-23, 1756-1771 (1987).

64. K.R. Karsch, M. Manser, W. Voelker, K.K. Haase, O. Ickrath and S. Duda, Percutaneous coronary excimer laser angioplasty: initial clinical results, Lancet Sept. 16 , 647-650 (1989).

65. F. Litvack, W. Grundfest, N. Eigler, D. Tsoi, T. Goldenberg, J. Laudenslager and J. Forrester, Percutaneous excimer laser coronary angioplasty, Lancet July 8, 102-103 (1989).

66. F. Litvack, J. Margolis, and T. Linnemeier, Percutaneous excimer laser coronary angioplasty: results of the first 110 procedures, J. Am. Coll. Cardiol. 15, 25A (1990).

67. K. Hohla, G. Laufer, G. Wollenek, R. Horvat, H.-W. Henke, M. Buchelt, G. Wuzi and E. Wolner, Simultaneous tissue identification and ablation with excimer laser, Proc. SPIE 908, 129 (1988).

68. S. Andersson-Engels, A. Gustafson, J. Johansson, U. Stenram, K. Svanberg and S. Svanberg, Laser-induced fluorescence used in localizing atherosclerotic lesions, Lasers Med. Sci. 4, 171-181 (1989).

69. Kittrell, R.L. Willet, C. de los Santos-Pacheo, N.B. Ratliff, J.R. Kramer, E.G. Malk and M.S. Feld, Diagnosis of fibrous arterial atherosclerosis using fluorescence, Appl. Opt. 24, 2280-2281 (1985).

70. J.J. Baraga, P. Taroni, Y.D. Park, K. An, A. Macstri, L.L. Tong, R.P. Rava, C. Kittrell, R.R. Dasari and M.S. Feld, Ultraviolet laser-induced fluorescence of human aorta, Spectrochim. Acta 45A, 95-99 (1989).

71. C.C. Hoyt, R.R. Richards-Kortum, B. Costello, B.A. Sachs, C. Kittrell, N.B. Ratliff, J.R. Kramer and M.S. Feld, Remote biomedical spectroscopic imaging of human artery wall, Lasers Med. Surg. 8, 1-9 (1988).

72. L.I. Deckelbaum, J.K. Lam, H.S. Cabin, K.S. Clubb and M.B. Long, Discrimination of normal and atherosclerotic aorta by laser induced fluorescence, Lasers Surg. Med. 7, 330-335 (1988).

73. A.A. Orayevsky, V.S. Letokhov, V.G. Omelyanenko, S.E. Ragimov, A.A. Belyaev and R.S. Akchurin, Laser spectral analysis of human atherosclerotic vessels, in: Laser Spectroscopy VIII, (W. Persson and S. Svanberg, eds.), pp. 370-371, Springer, Heidelberg, (1987).

74. P.S. Andersson, A. Gustafson, U. Stenram, K. Svanberg and S. Svanberg, Diagnosis of atherial atherosclerosis using laser induced fluorescence, Lasers Med. Sci. 2, 261-266 (1987).

75. S. Andersson-Engels, J. Johansson, U. Stenram, K. Svanberg and S. Svanberg, Time-resolved laser-induced fluorescence spectroscopy for enhanced demarcation of human atherosclerotic plaques, J. Photochem. Photobiol. B4, 363-369 (1990).

76. J. Aganauskiene, S. Andersson-Engels, C. Blomström-Lundquist, B. Olsson, U. Stenram, K. Svanberg and S. Svanberg, Characterization of myocardial tissue utilizing laser-induced fluorescence spectroscopy, to appear.

77. J. Johansson, S. Montán, S. Steen, U. Stenram, K. Svanberg and S. Svanberg, Fluorescence characterization of atherosclerotic plaques and normal vessel walls in vitro and in vivo, to appear.

78. S. Andersson-Engels, J. Johansson and S. Svanberg, The use of time-resolved fluorescence for diagnosis of atherosclerotic plaque and malignant tumours, Spectrochima Acta 46A, 1203-1210 (1990).

79. R.R. Alfano, C.H. Liu, W.L. Sha, H.R. Zhu, D.L. Akins, J. Cleary, R. Prudente and E. Cellmer, Lasers Life Sci. 4, 23 (1991).

80. J. J. Baraga,, M.S. Feld and R.P. Rava, Rapid near-infrared Raman spectroscopy of human tissue with a spectrograph and CCD detector, Appl. Spectr. 46, 187-190 (1992).

81. J.J. Baraga, M.S. Feld and R.P. Rava, In situ histochemistry of human artery using near infrared Fourier transform Raman spectroscopy, Proc. Natl. Acad. Sci. USA (1992).

82. T. Hirschfeld and B. Chase, Applied Spectroscopy 40, 133-139 (1986).

83. Reference to IR reflectance diagnostics of tissue

84. R. Berg, S. Andersson-Engels and S. Svanberg, Time-resolved transillumination imaging, in Optical Tomography, Ref. 85.

85. G. Müller et al. (eds), Optical Tomography, SPIE, Bellingham (1993)

86. K. Wårdell, A. Jacobsson, G.E. Nilsson, Imaging of tissue perfusion by dynamic light scattering, Trans. Biomed. Eng. IEEE, (1991).

87. I. Wang, K. Svanberg, S. Andersson-Engels, G.E. Nilsson, K. Wårdell and S. Svanberg, to appear.

88. M. Swift, D. Morrell, R.M. Massey and C.L. Chase, Incidence of cancer in 161 families affected by ataxia-telangiectasia, New Engl. J. Med. 325, 1831-1836 (1991).

89. R. J. Bartrum and H. C. Crow, Transillumination lightscanning to diagnose breast cancer: A feasibility study, Am. J Rad. 142, 409-414 (1984).

90. A. E. Profio, G. A. Navarro and O. W. Sartorius, Scientific basis of breast diaphanography, Med. Phys. 16, 60-65 (1989).

91. B. Monsees, J. M. Destouet and W. G. Totty, Light scanning versus mammography in breast cancer detection, Rad. 163, 463-465 (1987).

92. B. Chance, ed., Photon Migration in Tissue, Plenum, New York (1989).

93. S. Andersson-Engels, R. Berg, J. Johansson, K. Svanberg and S. Svanberg, Medical application of laser spectroscopy, in Laser Spectroscopy IX, (M. Feld, ed.), pp. 500-504, Academic Press, New York (1989).

94. S. Andersson-Engels, R. Berg, S. Svanberg and O. Jarlman, Time-resolved transillumination for medical diagnostics, Opt. Letters 15, 1179-1181 (1990).

95. S. Andersson-Engels, R. Berg and S. Svanberg, Effects of optical constants on time-gated transillumination of tissue and tissue-like media, J. Photochem. Photobiol. 16, 155-167 (1992).

96. R. Berg, O. Jarlman and S. Svanberg, Medical transillumination imaging using short pulse diode lasers, Appl. Opt. 32, 574-579 (1993).

97. R.R. Alfano, P.P. Ho and K.M. Yoo, Photons for prompt tumour detection, Phys. World 5, 37-40 (1992)

98. M. D. Duncan, R. Mahon, L. L. Tankersley and R. Reintjes, Time-gated imaging through scattering media using stimulated Raman amplification, Opt. Lett. 16, 1868-1870 (1991).

99. K. M. Yoo, Q. Xing and R. R. Alfano, Imaging objects hidden in highly scattering media using femtosecond second-harmonic-generation cross-correlation time gating, Opt. Lett. 16, 1019-1021 (1991).

100. J. Fishkin, E. Gratton, M. J. vandeVen and W. W. Mantulin, Diffusion of intensity modulated near-infrared light in turbid media, in: Time-Resolved Spectroscopy and Imaging of Tissue, (B. Chance, ed.), pp. 122-135, SPIE 1431 (1991).

101. S. L. Jacques, Principles of phase-resolved optical instruments, in: Future Trends in Biomedical Applications of Lasers, (L. O. Svaasand, ed.), pp. 143-153, SPIE 1525 (1991).

102. M. S. Patterson, J. D. Moulton, B. C. Wilson, K. W. Berndt and J. R. Lakowicz, Frequency-domain reflectance for the determination of the scattering and absorption properties of tissue, Appl. Opt. 30, 4474-4476 (1991).

103. M. Toida, T. Ichimura and H. Inaba, The first demonstration of laser computed tomography achieved by coherent detection imaging method for biomedical applications, IEICE Trans. E 74, 1692-1694 (1991).

104. K. G. Spears, J. Serafin, N. H. Abramson, X. Zhu and H. Bjelkhagen, Chrono-coherent imaging for medicine, IEEE Trans. Biomed. Eng. 36, 1210-1221 (1989).

105. H. Chen, Y. Chen, D. Dilworth, E. Leith, J. Lopez and J. Valdmanis, Two-dimensional imaging through diffusing media using 150-fs gated electronic holography techniques, Opt. Lett. 16, 487-489 (1991).

106. E. A. Swanson, D. Huang, M. R. Hee, J. G. Fujimoto, C. P. Lin and C. A. Puliafito, High-speed optical coherence domain reflectometry, Opt. Lett. 17, 151-153 (1992).

107. M.R. Hee, J.A. Izatt, J.M. Jacobson and J.G. Fujimoto, Femtosecond transillumination optical coherence tomography, Opt. Lett 18, 950-952 (1993).

108. B. Chance, J. S. Leigh, H. Miyake, D. S. Smith, S. Nioka, R. Greenfeld, M. Finander, K. Kaufmann, W. Levy, M. Young, P. Cohen, H. Yoshioka and R. Boretsky, Comparison of time-resolved and -unresolved measurements of deoxyhemoglobin in brain, Proc. Natl. Acad. Sci. USA 85, 4971-4975 (1988).

109. E.M. Sevick *et al.*, Anal Biochem., 195, 330 (1991).

110. D. T. Delpy, M. Cope, P. van der Zee, S. Arridge, S. Wray and J. Wyatt, Estimation of optical pathlength through tissue from direct time of flight measurement, Phys. Med. Biol. 33, 1433-1442 (1988).

111. J.P. Payne and J.W. Severinghaus (eds), Pulse Oximetry, Springer, Heidelberg (1986).

112. I.J. Bigio, T.R. Loree, T. Shimada, K. Story-Held, R.D. Glickman and R. Conn, Optical diagnostics based on elastic scattering: recent clinical demonstrations with the Los Alamos Biopsy System, in Proc. Biomedical Optics Europe '93, EUROPTO 2081, SPIE, Bellingham (1994).

FIGURE CAPTIONS

Fig. 1. Absorption properties of biological molecules: water, haemoglobin, melanin, haematoporphyrin derivative (HPD) and adenine (From Ref. 3).

Fig. 2. Energy level diagram for the HPD molecule and illustration of HPD fluorescence emission and energy transfer to oxygen molecules (From Ref. 7).

Fig. 3. Schematic diagram of tumor marking by sensitising molecules and the subsequent use for fluorescence diagnosis and photodynamic therapy (From Ref. 7).

Fig. 4. Fluorescence spectra for a) pure tissue constituent molecules and b) a number of tumor sensitising agents, accumulated in the same type of experimental rat tumor. (From Refs 13,14). Trp: tryptophan, HP: haematoporphyrin, DHE: dihaematoportphyrin ether (or Photofrin), PHE: polyhaematoporphyrin ester, BPD-MA: bensoporphyrin derivative - mono acid, TSPc: tetra sulphonated phtalocyanine.

Fig. 5. Laser-induced fluorescence spectra for an experimental tumor (a human colon adenocarcinoma inoculated in rat muscle), and normal surrounding tissue. The rat had been injected with a dose of haematoporphyrin derivative about 2 days before the investigation. Two excitation wavelengths, 337 and 405 nm, are chosen to illustrate the influence of the wavelength choice (From Ref. 23).

Fig. 6. Fluorescence data obtained in a scan across an experimental glioma (TCVC) in a rat injected with 1 mg/kg b.w. Photofrin 24 hours earlier. Laser-induced fluorescence spectra of tumor tissue and surrounding normal brain parenchyma are also shown. The background-free HPD-related signal is denoted A, while the total signal at 630 nm is denoted A' and the autofluorescence B. The dimensionless ratio A/B shows a strong contrast enhancement (From Ref. 30).

Fig. 7. Lay-out of a clinical fluorescence diagnostic system (From Ref. 31).

Fig. 8. Photograph of a clinical fluorosensor (From Ref. 31)..

Fig. 9. Fluorescence spectra and evaluated data from two different human malignant tumors and normal surrounding skin. To the left two fluorescence spectra and evaluated data from a scan across a basalioma 3 days after Photofrin incjection (2 mg/kg body weight). To the right two corresponding spectra and data from a scan across a breast carcinoma metastasis 1 day after Photofrin injection at the same dose (From Ref. 34,35).

Fig. 10. Fluorescence spectra for a papillary bladder tumor and normal surrounding mucosa for a patient, injected with a dose of 0.35 mg/kg bodyweight of Photofrin 48 hours prior to the investigation (top). Spectra are shown for 337 and 405 nm excitation. Spectra for mild and severe dysplasia are also included. (From Ref. 33).

Fig. 11. Plot of the value of the ratio I(630 nm)/I(500 nm) for a large number of locations in 21 patients studied using 405 nm excitation. The lower diagram is a magnification of low fluorescence values in the upper diagram. It can be specially noted, that dysplasia

consistently shows a larger value than normal tissue in each individual patient (From Ref. 33).

Fig. 12. Fluorescence spectra through different sections of a prostatic gland with a malignant tumor (From 36,37).

Fig. 13. Fluorescence spectra for a bronchial carcinoma and adjacent normal mucosa in a patient that had received a dose of Photofrin at a concentration of 1 mg/kg bodyweight 48 hours before the fluorescence investigation (From Ref. 36,38).

Fig. 14. Schematic diagram of PDT using ALA. By exchanging the laser wavelength to about 400 nm and recording the fluorescence from the tumor its extent can be clearly determined (From Ref. 47).

Fig. 15. Fluorescence data from scans through a basal cell carcinoma before (top) and after (bottom) PDT (60 J/cm2). An ALA cream had been topically applied over the tumor 6 hours prior to the fluorescence investigation (From Ref. 47,49).

Fig. 16. Diagram showing the basic construction of a multi-color fluorescence imaging system (From Ref. 53).

Fig. 17. Photograph of a clinical multi-color fluorescence system adapted for bronchoscope applications (Courtesy: Spectraphos AB, Lund).

Fig. 18. Imaging fluorescence recordings of a human T-cell lymphoma tumor in a patient that had been subject to topical ALA application 6 hours before the investigation. Individual images at 630, 600 and 470 nm are shown together with a processed image using the data in the three individual images (From Ref. 55).

Fig. 19. Photograph of the computer monitor screen showing a processed image of an experimental rat tumor of the same kind as was illustrated in Fig. 5. The excitation source was a nitrogen laser, operating at 337 nm (Ref. 55).

Fig. 20. Left: Imaging of a human basal cell carcinoma and a near-by benign naevus in a patient treated with topical ALA during 6 hours. The instrument shown in Fig. 17 was utilised. The processed tumor image is superimposed in the lower image on the normal color CCD output using a video mixer. Right: Corresponding images for a squamous cell carcinoma of the vocal cord. The images were taken through a straight endoscope. The patient had orally been given 7.5 mg/kg bodyweight 2 hours earlier. (Ref. 56).

Fig. 21. Schematic diagram of an atherosclerotically transformed vessel (From Ref. 61).

Fig. 22. Schematic diagram showing transluminal laser ablation of atherosclerotic plaque with three varieties of spectroscopic guidance: time-integrated fluorescence spectroscopy, time-resolved fluorescence monitoring and laser plasma emission spectroscopy (From Ref. 62).

Fig. 23. Absorption spectra for arterial and venous blood. Wavelength pairs with equal blood absorption are indicated (From Ref. 28).

Fig. 24. Demarcation of 5 different types of vessel wall using fluorescence spectroscopy. Data for 6 different demarcation criteria are shown. Criteria F5 and F6 are not affected by the presence of blood (From Ref. 28).

Fig. 25. Diagram showing differentiation of different kinds of myocardial tissue using fluorescence (From Ref. 76).

Fig. 26. Photograph of a fluorosensor for plaque monitoring employing photomultipliers observing fluorescence light, that has been selected for wavelength by interference filters (Courtesy: Spectraphos AB).

Fig. 27. Recording from the instrument shown in Fig. 26 for normal tissue and plaque in human aorta (From Ref. 77).

Fig. 28. Time-resolved fluorescence decay curves for a) atherosclerotic plaque and normal vessel wall, and b) an experimental tumor in an Photofrin-injected animal, and normal surrounding tissue (From Refs 75,78).

Fig. 29. Raman spectrum of a) fibrous plaque, b) atheromatous plaque and c) cholesterol monohydrate powder, excited with a 1064 nm CW Nd:YAG laser (From Ref. 81).

Fig. 30. a) Illustration of time-resolved signals received in elastic photon scattering measurements on tissue using two different geometries. b) Enhanced viewing through a scattering medium using detection of the first arriving photons in transillumination (From Ref. 84).

Fig. 31. Arrangement for scanning laser Doppler flowmetry for tissue (From Ref. 86).

Fig. 32. Normal photographs and imaging measurements of superficial blood perfusion in connection with ALA PDT. Recordings are shown for the following situations: a) before PDT, b) immediately after PDT. The arrow points to the marked area irradiated by the laser, c) one week after PDT, and d) 8.5 months after treatment (From Ref. 87).

Fig. 33. Transillumination scan through a human hand with data for the total time-integrated light and the early light (From Ref. 94).

Fig. 34. Two-dimensional transillumination scans through a resected breast sample containing a ductal carcinoma. The tumor clearly emerges in the early light, while it remains hidden in time-integrated monitoring (From Ref. 96).

Fig. 35. Set up for two-dimensional time-gated transillumination imaging through tissue, using a pulsed diode laser and time-correlated photon counting electronics (From Ref. 96).

Fig. 36. Experimental time-dispersion curves for light propagation through a 30 mm thick cuvette filled with a scattering and absorbing liquid. From the curves it is evident that the amount of early light is mainly influenced by the scattering and not by the absorption (From Ref. 95).

Table 1. Photosensitising drugs presently under different stages of clinical evaluation. The abbreviations frequently used and the approximate wavelength for PDT irradiation and fluorescence detection are given.

NAME	ABBREV.	λ nm
Photofrin	DHE	630
Bensoporphyrin	BPD	690
δ-amino levulinic acid	ALA	635
Mono aspartyl Chlorin e6	MACE	670
Tetra hydr.phenylchlorin	THPC	650
Zinc phtalocyanine	ZnPC	675
Tin ethyl etiopurpurin	SnET2	660